# *Resistance to PD1 blockade in the absence of metalloprotease-mediated LAG3 shedding*

HHS Public Access

Author manuscript

*Sci Immunol*. Author manuscript; available in PMC 2021 February 23.

Published in final edited form as:

*Sci Immunol*. 2020 July 17; 5(49): . doi:10.1126/sciimmunol.abc2728.

# Resistance to PD1 blockade in the absence of metalloprotease-mediated LAG3 shedding

**Lawrence P. Andrews**[1,2,3], **Ashwin Somasundaram**[1,2,3,4], **Jessica M. Moskovitz**[1,2,3], **Andrea L. Szymczak-Workman**[1], **Chang Liu**[1,2,3], **Anthony R. Cillo**[1,2,3], **Huang Lin**[5], **Daniel P. Normolle**[5], **Kelly D. Moynihan**[6,7], **Ichiro Taniuchi**[8], **Darrell J. Irvine**[6,7,9], **John M. Kirkwood**[3,4], **Evan J. Lipson**[10], **Robert L. Ferris**[2,3,11], **Tullia C. Bruno**[1,2,3], **Creg J. Workman**[1,2,3], **Dario A.A. Vignali**[1,2,3,†]

[1] Department of Immunology, University of Pittsburgh School of Medicine, Pittsburgh, PA.

[2] Tumor Microenvironment Center, UPMC Hillman Cancer Center, Pittsburgh, PA.

[3] Cancer Immunology and Immunotherapy Program, UPMC Hillman Cancer Center, Pittsburgh PA.

[4] Department of Medicine, Division of Hematology/Oncology, University of Pittsburgh School of Medicine, Pittsburgh, PA.

[5] Department of Biostatistics, University of Pittsburgh School of Public Health, Pittsburgh, PA.

[6] Department of Biological Engineering, Massachusetts Institute of Technology, Cambridge, MA.

[7] Koch Institute for Integrative Cancer Research, Massachusetts Institute of Technology, Cambridge, MA.

[8] RIKEN Center for Integrative Medical Sciences, Yokohama City, Kanagawa, Japan.

[9] Howard Hughes Medical Institute, Chevy Chase, MD.

[10] Department of Oncology, Sidney Kimmel Comprehensive Cancer Center, and Bloomberg-Kimmel Institute for Cancer Immunotherapy, Johns Hopkins University School of Medicine, Baltimore, MD.

[11] Department of Otolaryngology, University of Pittsburgh School of Medicine, Pittsburgh, PA.

[†] Corresponding author. dvignali@pitt.edu.

**Author contributions:** L.P.A. designed and performed all murine experiments and wrote the manuscript. A.S. and J.M.M. performed analysis of human subjects. A.L.S. designed and made the *Lag3*$^{NC.L/L}$ construct and generated the *Lag3*$^{NC.L/L}$ mice. C.L. assisted in preparation of RNAseq libraries and A.R.C. performed computational analysis of the RNAseq data. H.L. carried out statistical analysis and D.P.N. oversaw the statistical analyses. K.D.M., I.T. and D.J.I provided resources for murine experiments. J.M.K, E.J.L and R.L.F provided clinical material from human subjects. T.C.B. provided input in experiment design and data analysis of human subjects. C.J.W. assisted in designing the mouse construct, experiment design and data analysis of murine experiments. D.A.A.V. conceived the project, directed the research and wrote the manuscript. All authors edited and approved the manuscript.

**Data and materials availability:** The RNAseq data have been deposited in the Gene Expression Omnibus at the National Center for Biotechnology Information with the accession number GSE150991. The *Lag3*$^{NC.L/L}$ mice will be freely distributed to investigators at academic institutions for non-commercial research when an MTA is signed. These mice will also be distributed to commercial entities upon completion of a licensing agreement with the University of Pittsburgh. Individual requests for shipment of mice to AAALAC (Association for Assessment and Accreditation of Laboratory Animal Care International) accredited institutions will be honored. The recipient investigators should provide written assurance and evidence that the animals will be used solely in accord with their local IACUC review, that animals will not be distributed by the recipient without consent from the University of Pittsburgh, Office of Research, and that animals will not be used for commercial purposes.

## Abstract

Mechanisms of resistance to cancer immunotherapy remain poorly understood. Lymphocyte Activation Gene-3 (LAG3) signaling is regulated by A Disintegrin And Metalloprotease-10 (ADAM10) and ADAM17-mediated cell surface shedding. Here we show that mice expressing a metalloprotease-resistant, non-cleavable LAG3 mutant ($LAG3^{NC}$) are resistant to PD1 blockade and fail to mount an effective anti-tumor immune response. Expression of $LAG3^{NC}$ intrinsically perturbs $CD4^+$ T conventional ($T_{conv}$) cells, limiting their capacity to provide $CD8^+$ T cell help. Furthermore, the translational relevance for these observations is highlighted with an inverse correlation between high LAG3 and low ADAM10 expression on $CD4^+$ $T_{conv}$ cells in the peripheral blood of patients with head and neck squamous cell carcinoma (HNSCC), which corresponded with poor prognosis. This correlation was also observed in a cohort of patients with skin cancers, and was associated with increased disease progression after standard-of-care immunotherapy. These data suggest that subtle changes in LAG3 inhibitory receptor signaling can act as a resistance mechanism with a substantive effect on patient responsiveness to immunotherapy.

## Introduction

The immunotherapeutic blockade of inhibitory receptors (PD1, CTLA4) that promote tumor infiltrating lymphocyte (TIL) dysfunction has led to substantive improvements in objective responses across a wide variety of tumor types (1–5). However, only a small proportion of patients (10–30%) are responsive to these modalities as a monotherapy and a full understanding of the mechanisms of resistance remains elusive. LAG3 is an inhibitory receptor that co-expresses with PD1 on intratumoral T cells in several murine tumor models, and dual blockade synergistically limits tumor growth compared to either modality as a monotherapy (6). LAG3 co-expression with PD1 exemplifies a dysfunctional program of $CD8^+$ TIL with a reduced capacity to proliferate and produce cytokines (7). Thus, LAG3 is currently being targeted in the clinic by at least ten immunotherapeutics in combination with PD1/PDL1-targeting strategies to capitalize on expected synergy (8).

Altered metalloprotease activity and transmembrane protein shedding has been shown to have a dramatic effect on signaling activity and cell function for FasL (9, 10). LAG3 expression and consequent function is also regulated by cell surface shedding achieved by ADAM10 and 17 (a disintegrin and metalloprotease domain-containing protein). ADAM10/17 cleave LAG3 at the connecting peptide between the membrane proximal D4 domain and the transmembrane domain, releasing a monomeric soluble form of LAG3 (sLAG3). Importantly, sLAG3 that is released following metalloprotease-mediated shedding is not known to have any biological activity (11). However, previous *in vitro* studies have shown that preventing LAG3 shedding by generation of $LAG3^{NC}$ mutants impacts T cell function by enhancing inhibitory function (12).

Given these observations with $LAG3^{NC}$ mutants *in vitro*, we generated a conditional knock-in mouse that restricts $LAG3^{NC}$ to Cre-expressing cell populations, a unique tool to address the physiological relevance of LAG3 transmembrane shedding *in vivo*. As the impact of LAG3 shedding on anti-tumor immunity and subsequent response to immunotherapy is

unknown, we generated mice with LAG3$^{NC}$ restricted to T cells to assess the impact of LAG3 shedding in MC38 colon adenocarcinoma, a transplantable tumor model sensitive to anti-PD1 (6). We find that LAG3 shedding from the surface of CD4$^{+}$ conventional T cells ($T_{conv}$), and not CD8$^{+}$ T cells or CD4$^{+}$ regulatory T cells ($T_{regs}$), is essential for an effective anti-tumor response mediated by anti-PD1 immunotherapy in mouse models. Single-cell RNAseq analysis revealed the transcriptional relevance for LAG3 shedding on CD4$^{+}$ $T_{conv}$, as this population was transcriptionally altered as a result of LAG3$^{NC}$. Such CD4$^{+}$ $T_{conv}$ have reduced functionality with an impaired capacity for help, impacting CD8$^{+}$ T cell function that is required for tumor clearance. The translational relevance for these findings is highlighted by the inverse correlation between LAG3 and ADAM10 expression in the peripheral blood of treatment-naive patients with head and neck squamous cell carcinoma (HNSCC), demonstrating that LAG3 on CD4$^{+}$ $T_{conv}$ is a prognostic marker of poor disease outcome. Lastly, a cohort of patients with advanced skin cancer showed that disease progression following standard-of-care (SOC) anti-PD1/CTLA4 immunotherapy was associated with higher LAG3 expression on CD4$^{+}$ $T_{conv}$. Patients that responded to immunotherapy had a lower LAG3:ADAM10 ratio consistent with the phenotype of the LAG3$^{NC}$ mouse models described herein.

## Results

### Generation of a non-cleavable LAG3 conditional knock-in mouse

To assess the impact of LAG3 shedding on T cells, we generated a conditional knock-in mouse that allows for Cre recombinase-mediated, cell-type restricted expression of LAG3$^{NC}$. *Lag3* Exon 7, between the membrane-proximal D4 domain and the transmembrane domain, was replaced with an alternate version of the connecting peptide in which 12 amino acid residues were removed (LAG3$^{ESCP}$) and previously shown to be resistant to metalloprotease-mediated shedding *in vitro* (Fig. 1A; fig. S1A) (11, 12). In addition, EBFP and Ametrine were incorporated as fluorescent reporters for the transcriptional activity of *Lag3*$^{WT}$ (in the absence of Cre) and *Lag3*$^{NC}$ (in the presence of Cre), respectively (fig. S1B and C). *Lag3*$^{NC.L/L}$ mice were then crossed with several Cre recombinase mouse lines to facilitate cell type-restricted deletion to all T cells (CD4$^{Cre}$) (13), CD8$^{+}$ T cells (E8I$^{Cre.GFP}$) (14), CD4$^{+}$ T cells (tamoxifen-inducible ThPOK$^{CreERT2}$ [fig. S1D]), or regulatory T cells ($T_{regs}$; tamoxifen-inducible *Foxp3*$^{CreERT2.GFP}$ [fig. S1E]) (15). Release of sLAG3 *in vitro* was not detected following stimulation of T cells expressing both the *Lag3*$^{NC.L/L}$ floxed allele and Cre recombinase (fig. S1F). However, serum levels of sLAG3 were not substantively altered between LAG3$^{NC}$ mice and controls, due to other innate populations such as plasmacytoid DCs (pDCs) that are a major source of sLAG3 (fig. S1G) (16). Thus, our genetic system allows for the expression of LAG3 to be switched to a mutant non-cleavable form to selectively assess the impact of LAG3 shedding on the function of distinct T cell sub-populations within the tumor microenvironment (Fig. 1B).

### Restriction of LAG3$^{NC}$ to T cells impacts anti-PD1-mediated tumor regression

Two mouse models of cancer were used to assess the impact of LAG3$^{NC}$ on tumor growth: MC38, a model of adenocarcinoma, and B16-F10, a model of melanoma. No differences in primary tumor growth were observed between *Lag3*$^{NC.L/L}$CD4$^{Cre}$ mice and *Lag3*$^{NC.L/L}$

controls with either model, likely due to tumor-induced tolerance and checkpoint inhibition were already maximal (fig. S2A and B). Indeed, expression of the inhibitory receptors LAG3, PD1, TIM3 and CD244 (2B4) were unchanged on all T cell populations assessed, although TIGIT was elevated on $CD4^+Foxp3^-$ $T_{conv}$ and $CD8^+$ TIL from MC38-bearing *Lag3*$^{NC.L/L}$CD4$^{Cre}$ mice (fig. S2C to H). PD1 expression was also increased on $CD4^+Foxp3^-$ $T_{conv}$. No difference in proliferation, death and survival markers was observed in $CD4^+Foxp3^+$ $T_{reg}$, $CD4^+Foxp3^-$ $T_{conv}$ or $CD8^+$ MC38 TIL (fig. S2I to K). Furthermore, there was no difference in phosphorylated AKT or S6 by flow cytometry (fig. S2L and M).

We then assessed the impact of LAG3$^{NC}$ expression on an anti-tumor immune response following immunotherapy. We utilized a therapeutic anti-PD1 dosing regimen that results in ~30–40% of mice clearing MC38 tumors, as seen here in *Lag3*$^{NC.L/L}$ control mice and consistent with our previous observations (Fig. 1C and D; fig. S3A) (6). Strikingly, *Lag3*$^{NC.L/L}$CD4$^{Cre}$ mice exhibited substantially reduced sensitivity to anti-PD1 immunotherapy with <10% clearing tumors. This suggested that LAG3$^{NC}$ on T cells impaired the anti-tumor immune response elicited by blockade of the PD1 pathway.

To ensure that the restrictive impact of LAG3$^{NC}$ on anti-tumor immunity was not limited to this model, we evaluated two additional systems. First, using an MC38 re-challenge model in which the primary tumor was resected at day 12 and challenged with MC38 30 days later (fig. S3B), we showed that approximately half the *Lag3*$^{NC.L/L}$CD4$^{Cre}$ mice failed to clear MC38 while all the *Lag3*$^{NC.L/L}$ control mice were protected (Fig. 1E). Second, as B16 is refractory to anti-PD1 we utilized an immunotherapeutic regimen combining an amphiphile vaccine (Amph-vax) consisting of a gp100 antigen linked to a lipophilic albumin-binding tail by a solubility promoting polar polymer chain (gp100-vax) (17, 18) combined with anti-PD1 treatment. The combination of gp100-vax and anti-PD1 drives a strong immunotherapeutic response in C57BL/6 mice bearing a B16 line that overexpresses gp100 (B16-gp100) but not B16-F10, that expresses very low levels of gp100, compared with isotype control or a control amphiphile delivering a peptide derived from human papilloma virus (HPV)-derived cervical cancer antigen E7 (E7-vax) (fig. S3C and D). Interestingly, tumor reduction following combinatorial gp100-vax/anti-PD1 immunotherapy was not observed in *Lag3*$^{NC.L/L}$CD4$^{Cre}$ mice compared with *Lag3*$^{NC.L/L}$ controls, suggesting that LAG3$^{NC}$ on T cells blocks the anti-tumor immune response elicited by this therapeutic regimen (Fig. 1F). Taken together, these data suggest that LAG3$^{NC}$ limits T cell-mediated anti-tumor immunity in multiple mouse models.

## Transcriptomic analysis of LAG3$^{NC}$ on T cell populations in the context of PD1 blockade

To further understand which T cell population is selectively modulated by LAG3$^{NC}$ and is causative of the immunotherapeutic resistance shown in this model, we assessed the transcriptional profiles of T cells isolated from MC38 tumors pooled from *Lag3*$^{NC.L/L}$ and *Lag3*$^{NC.L/L}$CD4$^{Cre}$ mice following anti-PD1 immunotherapy, or isotype control, using single cell transcriptomic analysis (single-cell RNAseq; fig. S4A). We initially utilized a single-cell RNAseq analysis pipeline (Methods) to embed all cells in a 2-dimensional fast interpolation-based t-distributed stochastic neighborhood embedding (FltSNE(19)) and performed clustering and differential gene expression analysis to classify cell types based on canonical

markers (e.g. clusters with high expression of *Cd3d* and *Cd8a* were classified as $CD8^+$ T cells). We identified $CD8^+$ T cells, $CD4^+Foxp3^+$ $T_{reg}$ and $CD4^+Foxp3^-$ $T_{conv}$ lineages (Fig. 2A). The frequencies of these T cell subsets recovered bioinformatically were similar to those identified by flow cytometry, with $CD4^+Foxp3^+$ $T_{reg}$ as the largest subpopulation recovered (fig. S4B). To assess the magnitude of transcriptional differences between cell types and treatment conditions, we measured the distance between experimental groups in high dimensional space using the Bhattacharyya distance (BD) for the three T cell populations identified (Fig. 2B; Table 1). This analysis surprisingly revealed the greatest transcriptional differences in the $CD4^+Foxp3^-$ $T_{conv}$ population, specifically when comparing the isotype versus anti-PD1 treatment in the $Lag3^{NC.L/L}CD4^{Cre}$ mice. This finding suggests that $CD4^+Foxp3^-$ $T_{conv}$ in the $Lag3^{NC.L/L}CD4^{Cre}$ mice change more than other populations following anti-PD1 therapy. Further, this analysis also revealed subtle differences in the $CD8^+$ T cell population, although these differences were largely a result of anti-PD1 treatment across both genotypes. Surprisingly, this analysis revealed that the $CD4^+Foxp3^+$ $T_{reg}$ population was largely similar between samples.

To address the transcriptional differences of $CD4^+Foxp3^-$ $T_{conv}$ between groups, we bioinformatically isolated and re-clustered this population to identify a total of seven clusters, projected by FltSNE (Fig. 2C; fig. S5A and B). To illustrate the enrichment of different genotypes and treatment conditions across clusters, we generated heat maps to assess the scaled enrichment of sample across the clusters (Fig. 2D). Since $CD4^+Foxp3^-$ $T_{conv}$ changed most in the $Lag3^{NC.L/L}CD4^{Cre}$ mice following anti-PD1 treatment, we sought to evaluate the transcriptional profile associated with this group. We found that cells from Cluster 2 had the highest scaled enrichment for this group, representing a higher than anticipated frequency of cells, compared to anti-PD1-treated $Lag3^{NC.L/L}$ controls (fig. S5C). Conversely, Cluster 1 was the most highly enriched cluster in the comparator group ($Lag3^{NC.L/L}$ + anti-PD1). Gene set enrichment analysis revealed that Cluster 2 was driven by several interferon signaling pathways (Fig. 2E). Furthermore, three members of the IFITM family that are expressed in T cells (*Ifitm1–3)* were shown to be highly upregulated (fig. S5D). Recently it has been shown that IFITM proteins regulate Th1 differentiation as *Ifitm*-deficient $CD4^+$ T cells have higher expression of Th1-assoicated genes, including IFNγ (20, 21). This suggests that $CD4^+$ T cells from $Lag3^{NC.L/L}CD4^{Cre}$ mice treated with anti-PD1 may be less Th1-like than the $Lag3^{NC.L/L}$ group.

Bioinformatically isolating $CD4^+Foxp3^+$ $T_{regs}$ and re-clustering identified nine clusters (fig. S6A). Fewer differences for enriched clusters between experimental groups were apparent for this population, however Cluster 8 was enriched following anti-PD1 treatment in $Lag3^{NC.L/L}CD4^{Cre}$ mice and also had higher expression of interferon signaling pathways (fig. S6B to F). Assessment of the transcriptional differences of $CD8^+$ T cells following re-clustering showed differences when assessing enrichment of the six clusters identified (fig. S7A to F). Taken together, this analysis suggests that the largest transcriptional differences exist in the $CD4^+Foxp3^-$ $T_{conv}$ compartment with respect to the difference between wild-type and $LAG3^{NC}$ experimental groups.

## Lag3$^{NC}$ intrinsically impacts CD4$^{+}$ T cell functionality

To assess whether LAG3$^{NC}$ on CD4$^{+}$ T cells impacted tumor clearance with immunotherapeutic blockade, we utilized *Lag3*$^{NC.L/L}$ThPOK$^{CreERT2}$ mice in which LAG3$^{NC}$ was restricted to CD4$^{+}$ T cells following tamoxifen administration. As with *Lag3*$^{NC.L/L}$CD4$^{Cre}$ animals, tamoxifen-administered *Lag3*$^{NC.L/L}$ThPOK$^{CreERT2}$ mice exhibited reduced survival following MC38 inoculation when treated with anti-PD1 compared with control mice (Fig. 3A and B; fig. S8A). To further interrogate the role of LAG3$^{NC}$ on TIL functionality, cytokines were assessed by flow cytometry at day 14 following MC38 inoculation, stratified by responsiveness to anti-PD1 compared to isotype control (responders and non-responders) (fig. S8B). An increase in IFN$\gamma^{+}$ TNF$\alpha^{+}$ CD4$^{+}$Foxp3$^{-}$ T$_{conv}$ when *Lag3*$^{NC.L/L}$ controls were treated with anti-PD1 was not evident in *Lag3*$^{NC.L/L}$CD4$^{Cre}$ mice (Fig. 3C; fig. S8C and D). Conversely KLRG1, which is reduced following anti-PD1 and has been shown to inhibit CD4$^{+}$ T cell responses (22), was increased on CD4$^{+}$Foxp3$^{-}$ T$_{conv}$ cells expressing LAG3$^{NC}$ (fig. S8E). Indeed, TNFα-producing CD4$^{+}$ T$_{conv}$ cells, more evident in *Lag3*$^{NC.L/L}$ control mice, were KLRG1-negative (fig. S8F). Moreover, an increase of IL-2 production was observed within CD4$^{+}$Foxp3$^{-}$ TIL of *Lag3*$^{NC.L/L}$ control animals receiving anti-PD1, which was not evident in *Lag3*$^{NC.L/L}$CD4$^{Cre}$ mice (Fig. 3D). CD4$^{+}$Foxp3$^{-}$ TIL were also more proliferative by Ki67 staining and BrdU incorporation following anti-PD1 treatment in *Lag3*$^{NC.L/L}$ controls, than in *Lag3*$^{NC.L/L}$ CD4$^{Cre}$ mice (Fig. 3E). Whereas a statistically significant increase in cleaved caspase-3 (cCasp3), but not Bcl2, in CD4$^{+}$Foxp3$^{-}$ TIL was shown in *Lag3*$^{NC.L/L}$CD4$^{Cre}$ mice, compared to *Lag3*$^{NC.L/L}$ controls, there was no statistical difference between these groups following anti-PD1 treatment (fig. S8G and H).

To further investigate whether the LAG3$^{NC}$ phenotype on CD4$^{+}$ T cells selectively impacts CD4$^{+}$Foxp3$^{-}$ T$_{conv}$ rather than CD4$^{+}$Foxp3$^{+}$ T$_{reg}$, we used *Lag3*$^{NC.L/L}$*Foxp3*$^{CreERT2.GFP}$ mice which restricts LAG3$^{NC}$ expression to CD4$^{+}$Foxp3$^{+}$ T$_{regs}$ following tamoxifen administration. In contrast to *Lag3*$^{NC.L/L}$ThPOK$^{CreERT2}$ mice, anti-PD1-treated *Lag3*$^{NC.L/L}$*Foxp3*$^{CreERT2.GFP}$ mice exhibited similar tumor clearance to their tamoxifen-treated controls (*Foxp3*$^{CreERT2}$ and *Lag3*$^{NC.L/L}$) with consequent improved survival (fig. S9A to C). Moreover, proliferation and frequency of CD4$^{+}$Foxp3$^{+}$ T$_{regs}$ was unchanged between *Lag3*$^{NC.L/L}$CD4$^{Cre}$ and control mice treated with anti-PD1 or isotype (fig. S9D and E). Bcl2 and cCasp3 expression was also unchanged between experimental groups, although cCasp3 was significantly increased in T$_{regs}$ isolated from isotype-treated *Lag3*$^{NC.L/L}$CD4$^{Cre}$ mice compared with controls (fig. S9F and G). Taken together, these data suggest that LAG3$^{NC}$ selectively impacts CD4$^{+}$Foxp3$^{-}$ T$_{conv}$ and not CD4$^{+}$Foxp3$^{+}$ T$_{regs}$ within the tumor, which in turn limits an effective anti-tumor immune response following anti-PD1 immunotherapy.

To confirm the selective role for LAG3$^{NC}$ on CD4$^{+}$Foxp3$^{-}$ T$_{conv}$ cells, we immunized *Lag3*$^{NC.L/L}$, *Lag3*$^{NC.L/L}$CD4$^{Cre}$ or *Lag3*$^{NC.L/L}$E8I$^{Cre.GFP}$ mice with MOG$_{35–55}$ to induce experimental autoimmune encephalomyelitis (EAE), a CD4$^{+}$ T helper cell-mediated disease model. *Lag3*$^{NC.L/L}$CD4$^{Cre}$ mice exhibited a reduced severity of EAE compared to *Lag3*$^{NC.L/L}$ controls and *Lag3*$^{NC.L/L}$E8I$^{Cre.GFP}$ mice (Fig. 3F). As a result of LAG3$^{NC}$, there is a reduction of pathogenic IFN$\gamma^{+}$IL17$^{+}$GMCSF$^{+}$ CD4$^{+}$Foxp3$^{-}$ T$_{conv}$ isolated from the

brain (day 15 following immunization) (Fig. 3G). Moreover, this T cell population showed a selective reduction of proliferation in *Lag3*$^{NC.L/L}$CD4$^{Cre}$ mice compared to *Lag3*$^{NC.L/L}$ controls, which was not significant in $T_{regs}$ or CD8$^+$ T cells isolated from the brain (Fig. 3H). Taken together, these results show a selective role for LAG3$^{NC}$ mediating CD4$^+$ Foxp3$^-$ $T_{conv}$ functionality and proliferation in two different disease models.

## LAG3$^{NC}$ extrinsically modulates effector CD8$^+$ T cell functionality

We had initially predicted that LAG3$^{NC}$ would have a dominant effect on CD8$^+$ T cells, particularly given that this population has the greatest expression of LAG3 within the TIL compartment and their central role in anti-tumor immunity (8). Our transcriptional analysis had shown that any differences observed with CD8$^+$ TIL were primarily due to the impact of anti-PD1 treatment rather than LAG3$^{NC}$ expression. We were surprised to find that *Lag3*$^{NC.L/L}$E8I$^{Cre.GFP}$ mice exhibited similar tumor regression and survival to controls, suggesting that LAG3$^{NC}$ expression on CD8$^+$ T cells did not impact response to anti-PD1 (Fig. 4A and B; fig. S10A). To further interrogate the role of LAG3$^{NC}$, MC38 TIL were assessed by flow cytometry at day 14 following inoculation, stratified by responsiveness to anti-PD1 compared to isotype (fig. S10B). Although an intrinsic LAG3$^{NC}$ CD8$^+$ T cell phenotype was not observed in MC38 tumor-bearing, anti-PD1-treated *Lag3*$^{NC.L/L}$E8I$^{Cre.GFP}$ mice, IFNγ/TNFα release from re-stimulated CD8$^+$ TIL isolated from *Lag3*$^{NC.L/L}$CD4$^{Cre}$ mice was reduced compared to controls when treated with anti-PD1 (Fig. 4C; fig. S10C and D). In contrast, CD8$^+$ TIL isolated from *Lag3*$^{NC.L/L}$E8I$^{Cre.GFP}$ mice do exhibit increased IFNγ/TNFα release following anti-PD1 treatment despite LAG3$^{NC}$ expression on CD8$^+$ T cells, confirming that this is a LAG3$^{NC}$ cell-extrinsic effect. No differences in proliferation or death and survival were observed in CD8$^+$ T cells (fig. S10E to G).

CD4$^+$Foxp3$^-$ $T_{conv}$ have been shown to promote the effector function of CD8$^+$ TIL to produce IFNγ and subsequently enhance anti-tumor immunity (23). To provide further support for a cell-extrinsic effect on CD8$^+$ T cells, gp100-specific Thy1.1$^+$ pmel CD8$^+$ T cells were adoptively transferred into B16-gp100 tumor-bearing *Lag3*$^{NC.L/L}$ or *Lag3*$^{NC.L/L}$CD4$^{Cre}$ hosts, which also received anti-PD1 (fig. S11A). When transferred into *Lag3*$^{NC.L/L}$CD4$^{Cre}$ hosts, tumor size was larger compared to *Lag3*$^{NC.L/L}$ control hosts and Thy1.1$^+$ pmel cells isolated from the tumor produced less IFNγ (Fig. 4D and E). Size of tumor and cytokine release had no relationship to the extent of pmel infiltration (fig. S11B to E). Taken together, these data suggest that LAG3$^{NC}$ extrinsically impacts CD8$^+$ T cell-mediated clearance of tumors following PD1 blockade.

## ADAM-mediated cell surface shedding of LAG3 promotes anti-tumor immunity

The observations above are a consequence of preventing LAG3 shedding by expression of a non-cleavable LAG3 mutant. To assess the effect of ADAM-mediated cell surface shedding of LAG3, the expression of *Adam10* in sorted T cell populations isolated from B16-F10 tumor-bearing *Foxp3*$^{Cre\text{-}YFP}$ mice was assessed by quantitative real-time polymerase chain reaction (qPCR) and compared to peripheral T cell populations (fig. S12A). CD8$^+$ T cells isolated from B16-F10 tumors, but not CD4$^+$ $T_{conv}$ or $T_{reg}$ populations, have reduced *Adam10* expression compared to the periphery. This may explain why CD8$^+$ TIL have the

highest amount of LAG3 expression and why a phenotype was not observed in *Lag3*$^{NC.L/L}$E8I$^{Cre.GFP}$ mice.

To determine if the phenotype observed in *Lag3*$^{NC.L/L}$CD4$^{Cre}$ mice is synonymous with ADAM-metalloprotease enzymatic activity, an ADAM10 inhibitor (GI254023X) was utilized that limits LAG3 shedding from CD4$^{+}$Foxp3$^{-}$ $T_{conv}$ and CD8$^{+}$ T cells *in vitro* (fig. S12B and C) (24). To investigate the effect of ADAM10-mediated LAG3 shedding *in vivo*, C57BL/6 mice were subcutaneously implanted with Alzet osmotic pumps releasing GI254023X (20mg/kg/d) over 14 days, which resulted in the reduction of sLAG3 in sera by 30% compared to mice receiving vehicle control (fig. S12D). Following anti-PD1 treatment, mice receiving GI254023X exhibited a reduced percentage of IFN$\gamma^{+}$-producing CD8$^{+}$ TIL versus controls, a reduction that was comparable to *Lag3*$^{NC.L/L}$CD4$^{Cre}$ mice, with a trend towards larger tumors (fig. S12E and F). This supports the notion that the phenotype exhibited by expression of LAG3$^{NC}$ on T cells is due to limiting ADAM10 metalloprotease-mediated LAG3 shedding.

## Low LAG3:ADAM10 ratio on conventional CD4$^{+}$ T cells is indicative of patient survival and responsiveness to PD1 blockade

Although substantial clinical success has been achieved with PD1/PDL1-targeting agents, the majority of cancer patients do not respond to checkpoint blockade, and so targeting co-expressed inhibitory receptors such as LAG3 has been suggested to enhance objective response rates (8). To understand the clinical relevance of the relationship between LAG3 and ADAM10 expression, we assessed CD4$^{+}$Foxp3$^{-}$ $T_{conv}$, CD4$^{+}$Foxp3$^{+}$ $T_{reg}$ and CD8$^{+}$ T cell populations isolated from fresh tumor tissue and matched peripheral blood lymphocytes (PBL) from treatment-naïve patients with metastatic melanoma (Table 2). While healthy donor PBL did not express surface LAG3, remarkably, a subset of melanoma patients did show enhanced LAG3 expression on both CD4$^{+}$Foxp3$^{-}$ $T_{conv}$ and CD4$^{+}$Foxp3$^{+}$ $T_{reg}$ populations in peripheral blood, with expression further enhanced in corresponding TIL populations (fig. S13A to D). CD8$^{+}$ T cells from patient peripheral blood showed a minimal LAG3 expression profile, although this is still greatly enhanced in the tumor compartment (fig. S13E and F). There was also heterogenous expression of ADAM10 in patient PBL, particularly on CD4$^{+}$ T cell populations (fig. S13G to L). We next assessed the relationship between LAG3 and ADAM10 by paired analysis. For CD4$^{+}$ T cell populations in tumor and peripheral blood, a group of patients with higher LAG3 expression inversely correlated with lower ADAM10 expression (fig. S13M to R).

To further understand the clinical relevance of the dichotomy observed between LAG3 and ADAM10, particularly on CD4$^{+}$Foxp3$^{-}$ $T_{conv}$, peripheral blood isolated from a second cohort of patients with advanced metastatic melanoma and other skin cancers was assessed who had received SOC anti-PD1 or anti-PD1/CTLA4 immunotherapy (Table 3). Patients were stratified by response to treatment according to RECIST 1.1 criteria, consisting of 18 patients who showed either initial partial (PR) or complete response (CR) and 19 patients with initial disease progression (PD). While there was no difference in LAG3 expression on T cell populations before and after immunotherapy in the cohort of patients that responded to treatment, there was a statistically significant increase in LAG3 expression on

$CD4^+Foxp3^-$ $T_{conv}$ in the cohort of patients that progressed, which was not evident for $CD4^+Foxp3^+$ $T_{regs}$ or $CD8^+$ T cells (Fig. 5A; fig. S14A to E). Although, changes in ADAM10 expression before and after treatment were not significant (fig. S14F to H), paired analysis with LAG3 shows a similar dichotomy of expression compared to the previous cohort (Fig. 5B; fig. S14I and J). As a result, the LAG3:ADAM10 ratio was found to be statistically increased on $CD4^+Foxp3^-$ $T_{conv}$ in the PBL of patients that progressed following treatment, but not on $CD4^+Foxp3^+$ $T_{regs}$ or $CD8^+$ T cells (Fig. 5C; fig. S14K and L). This suggests that LAG3 on $CD4^+$ $T_{convs}$, in which level of expression is modulated by ADAM10-mediated cell surface shedding, acts as a primary resistance mechanism during immunotherapy and is associated with poor responsiveness to treatment.

The clinical relevance for LAG3 and ADAM10 expression on $CD4^+$ $T_{conv}$ PBL was further supported by analysis of a third patient cohort with a different tumor type - treatment-naïve HNSCC (Table 4). In previous studies, LAG3 over-expression on TIL has been shown to be a prognostic factor correlating to higher tumor pathological grades (25–27). Similar observations are shown for treatment-naïve HNSCC patients compared to the metastatic melanoma cohort, with elevated LAG3 surface expression on $CD4^+$ T cell populations in patient peripheral blood compared to healthy donors (fig. S15A to C). Again, there is heterogeneous expression of ADAM10 and ADAM17 on patient PBL, although this is inversed correlated to LAG3 on each cell type (fig. S15D to L). HPV has been identified as the causative agent of a subgroup of HNSCC patients, which have higher responsiveness towards PD1 blockade (28). Interestingly, patients with HPV-positive status show minimal expression of LAG3 on $CD4^+$ T cell populations in peripheral blood (fig. S15M to O).

Given the heterogeneous level of LAG3 expression that was also evident for the HNSCC patient cohort, we wanted to further confirm the clinical relevance of ADAM-mediated cell surface shedding of LAG3 by analyzing a second cohort (fourth in total analyzed in this study) of frozen-banked treatment-naïve HNSCC patient PBL samples consisting of 25 early stage disease (T1, T2, T3 and/or N0, N1) and 25 advanced disease cases (T4 and/or N2B, N2C, N3) for whom clinical outcome data were available (Table 5). LAG3 expression on $CD4^+Foxp3^-$ $T_{conv}$, but not $CD4^+Foxp3^+$ $T_{reg}$ and $CD8^+$ T cells in peripheral blood, was associated with advanced stage disease (Fig. 5D). Despite the difference in LAG3 surface expression on $CD4^+$ T cell populations, sLAG3 in patient sera was also unchanged suggesting this may not be a useful clinical biomarker as there are other cell types which shed LAG3, as in mice (fig. S16A). In this cohort, ADAM10 expression was also statistically reduced on $T_{regs}$ in patients with advanced disease (fig. S16B). As previously shown, the heterogeneity of LAG3 expression in PBL inversely correlated with ADAM10 expression in $CD4^+$ T cell populations, but not $CD8^+$ T cells (Fig. 5E; fig. S16C and D). Assessing all parameters within the advanced disease patient cohort showed that low (<23.5%) LAG3 expression on $CD4^+Foxp3^-$ $T_{conv}$, was the best predictor for survival, with poor prognosis for patients with high (≤23.5%) LAG3 expression (fig. S16E). As $CD4^+Foxp3^-$ $T_{conv}$ with high LAG3 expression had relatively low ADAM10 expression, patients with a low LAG3:ADAM10 ratio (<0.3865) had better survival outcome than patients with a high LAG3:ADAM10 ratio (≤0.3865) (Fig. 5F).

## Discussion

Overall our study suggests four key points. First, ADAM-mediated cell surface shedding of LAG3 is important for effective anti-tumor immune responses, as demonstrated *in vivo* with a conditional knock-in mouse model in which clinical relevance of these observations is exemplified, suggesting that LAG3 acts as a mechanism of primary resistance in patients with advanced cancer receiving checkpoint blockade therapy, and that LAG3:ADAM10 expression on $CD4^+Foxp3^-$ $T_{conv}$ may act as a systemic prognostic biomarker in a select group of patients. The potential importance of additional co-inhibitory receptors beyond PD1, such as LAG3, that impact responsiveness to immunotherapy, with a subsequent impact on disease progression and survival is evident, particularly given that anti-PD1 as a monotherapy only benefits a proportion of patients.

Second, our observations highlight the surprising impact that limiting ADAM-mediated cell surface shedding of an inhibitory receptor can have on immune responses, in general, and responsiveness to immunotherapy, specifically. Indeed, the resistance demonstrated to PD1 blockade in preclinical models and the relationship between a high LAG3:ADAM10 ratio and poor prognosis in HNSCC and responsiveness to immunotherapy in melanoma patients highlight altered LAG3 shedding as a potential resistance mechanism.

Third, we were surprised to find that limiting LAG3 shedding could impact T cells function without demonstrably impacting cell surface expression as determined by flow cytometry. We speculate that as ADAM10 is recruited to the immunological synapse during T cell activation, it is in this context that the resistance of LAG3 to shedding becomes functionally impactful (29, 30).

Fourth, our results demonstrate the importance of $CD4^+Foxp3^-$ $T_{conv}$ cells in driving a protective immune response following immunotherapy despite preoccupation in the field with checkpoint blockade directly re-invigorating $CD8^+$ T cells or disabling $CD4^+Foxp3^+$ $T_{regs}$. Indeed, $CD4^+Foxp3^-$ $T_{conv}$ cells may serve as a nexus for more resistance mechanisms to effective immunotherapy than previously appreciated.

## Materials and Methods

### Study Design

This study aimed to investigate whether LAG3 shedding from T cell populations is required to generate sufficient anti-tumor immune responses necessary for tumor clearance *in vivo*. We generated a conditional knock-in mouse that renders a non-cleavable form of LAG3 ($LAG3^{NC}$) to Cre-expressing T cell populations. We used *in vitro* and *in vivo* assays to validate the mice by flow cytometry and enzyme-linked immunosorbent assay (ELISA). We evaluated the effect of $LAG3^{NC}$ on tumor growth and functionality of intratumoral T cells using flow cytometry. Tumors were measured every 3 days with digital calipers and tumor volume calculated blinded and randomized for treatment group. Mice were removed from study when tumor growth reached a mean diameter of 1.5cm or when necrosis was observed. The number of experimental replicates as well as statistical methods are described

in the figure legends. Samples were double-blinded or randomized during experiments or analyses.

All human samples (peripheral blood and tumor) were obtained after approval from the Institutional Review Board of the University of Pittsburgh Medical Center and Johns Hopkins University School of Medicine. All individuals were recruited with written informed consent.

## Cell Lines and Reagents

B16-F10 cells were obtained from M.J. Turk (Dartmouth College, New Hampshire). B16-gp100 cells were obtained from P.M. Sondel (University of Wisconsin, Wisconsin). MC38 cells were obtained from J.P. Allison (M.D. Anderson Cancer Center, Texas). B16 cell lines were cultured in complete Roswell Park Memorial Institute (RPMI) media (Lonza) and MC38 cell lines were cultured in complete Dulbecco's Modified Eagle's Medium (DMEM, Lonza), both supplemented with 10% FBS, 100units/ml penicillin, 100μg/ml streptomycin, 2mM glutamine, 1mM pyruvate, 5mM HEPES, 100μM non-essential amino acids and 2-ME. B16-gp100 cells were cultured with the addition of 0.8mg/ml geneticin (ThermoFisher Scientific). All cell lines and assay cultures were maintained at 37°C and 5% $CO_2$.

Amphiphile-CpG (Amph-CpG) was produced as previously described (17). Cysteine-modified amphiphilic-peptides for gp100 (CAVGALEGPRNQDWLGVPRQL) and HPV-$E7_{43–62}$ (IDGPAGQAEPDRAHYNIVTFC) were conjugated to maleimide-DSPE-PEG-2000 in dimethyl formamide at The Peptide Synthesis Core Facility, Northwestern University. Bioconjugations were purified by reverse phase HPLC and peptide amphiphiles were characterized by MALDI-TOF mass spectrometry. The peptide conjugates were then diluted in 10x $ddH_2O$ and lyophilized into powder, re-dissolved in DMSO and stored at −80°C.

## Mice

C57BL/6, $Rosa26^{LSLtdTomato}$ and pmel mice were obtained from Jackson Laboratories. $CD4^{Cre}$ mice were obtained from P. Brindle (St. Jude Children's Research Hospital, Tennessee). $E8I^{Cre.GFP}$ were previously described (14). $ThPOK^{CreERT2}$ mice were established in the laboratory of I. Taniuchi by using a minigene transgene construct which was constructed by replacing Cre cDNA with CreERT2 cDNA in the Thpok-Cre construct (31). *Foxp3*$^{CreERT2.GFP}$ and *Foxp3*$^{Cre.YFP}$ mice were obtained from A.Y. Rudensky (Memorial Sloan Kettering Cancer Center, New York). $LAG3^{-/-}$ mice were obtained from Y-H Chen (Stanford University, California) with permission from C. Benoist and D. Mathis. $LAG3^{NC}$ mice were generated in house as detailed below. All animal experiments were performed in the American Association for the Accreditation of Laboratory Animal Care-accredited, specific-pathogen-free facilities in Division of Laboratory Animal Resources, University of Pittsburgh School of Medicine. Female and male mice were used. Mice were used for studies when 4–8 weeks old, except for EAE studies which were used when 8–12 weeks old. Animal protocols were approved by the Institutional Animal Care and Use Committees of the University of Pittsburgh.

## Generation of LAG3$^{NC}$ Mice

The *Lag3*$^{NC.L/L}$ targeting construct was generated using standard recombineering methods (32). Initially, 15.4 kb of the *Lag3* locus were retrieved from a BAC plasmid (RP23–408H4) and a Loxp-Neo-Loxp cassette inserted 195bp upstream of exon 7. The Neo was removed via Cre-mediated recombination leaving a single Loxp and an *Eco*RI restriction site (inserted into the intron of the retrieved *Lag3* locus). The following was then inserted: a 'self cleaving' T2A peptide sequence followed by EBFP2 prior to the stop codon of *Lag3* in exon 8, a *Xba*I restriction site with a Frt-Neo-Frt-Loxp cassette 261bp from the end of exon 8, 160bp of the splice acceptor site of *Lag3* intron 6 followed by alternate versions of exons 7 and 8 of *Lag3* that lack the connecting peptide (HSARRISGDLKG) and has the 'self cleaving' P2A peptide followed by Ametrine inserted prior to the stop codon. The linearized targeting construct was electroporated into JM8A3.N1 embryonic stem cells and neomycin-resistant clones were screened by southern blot analysis using *Eco*RI and *Xba*I restriction digests for the 5' and 3' ends, respectively. Correctly targeted clones were 100% normal diploid by karyotype analysis and were injected into C57BL/6 blastocysts. Chimeric mice were mated to C57BL/6 mice and transmission of the targeted allele verified by PCR. The mice were crossed with actin flipase mice to remove the Neo cassette.

## Human T cell populations

**Patients and specimens—**All patients were seen either in the Division of Hematology/Oncology at University of Pittsburgh Medical Center (UPMC) (Cohort A), or in the Department of Oncology at the Sidney Kimmel Comprehensive Cancer Center (SKCCC) and Bloomberg-Kimmel Institute for Cancer Immunotherapy at Johns Hopkins University School of Medicine (Cohort B) and the Department of Otolaryngology at UPMC (Cohort C and D) and consented for participation in a specimen collection research protocol at their respective institutions. Cohort A consisted of matched PBL and TIL (n=14) thawed from patients with metastatic melanoma from the Division of Oncology at UPMC. Cohort B consisted of banked PBL samples collected from patients with metastatic melanoma or other skin cancers before beginning checkpoint blockade therapy (including anti-PD1 therapy or the combination of anti-PD1 and anti-CTLA4 therapy) and collected again at the time of the patient's initial scans nearing 12 weeks on checkpoint blockade therapy. Patients in this cohort were responders (CR or PR) (n=18), or progressors (PD) (n=19) from SKCCC. Response and progression was determined by RECIST 1.1 criteria. Cohort C consisted of tumor and PBL samples from HNSCC patients with primary disease (n=29). Patients that presented to UPMC with biopsy proven HNSCC that elected to undergone radiation or chemotherapy and radiation that elected to participate in the research protocol donated blood at time of surgery or at time of clinic visit. Tumor tissue from the primary site of disease was obtained from patients undergoing both biopsy and definitive surgical therapy. Cohort D consisted of a cohort of banked PBL samples from HNSCC patients with both early stage (n=25) and advanced (n=25) disease for correlation with disease progression and survival.

**Isolation of Patient Blood and TIL samples.:** Patient blood samples were drawn into heparinized tubes and centrifuged on a Ficoll-Hypaque gradient (GE Healthcare Bioscience). Peripheral blood lymphocytes (PBL) were recovered and washed in RPMI media.

Tumor samples were washed in an antibiotic medium of RPMI with penicillin-streptomycin and amphotericin B for 30 minutes. Tissue was then mechanically digested and passed through a 100μm filter. Tumor infiltrating lymphocytes (TIL) were washed and isolated. Bulk TIL and PBL were stained for flow cytometric analysis.

## Antibodies and Flow Cytometry

For murine experiments, single cell suspensions were stained with antibodies against TCRβ (H57–597; eBioscience), CD4 (GK1.5; Biolegend), CD8α (53–6.7; Biolegend), CD8β (YTS156.7.7; Biolegend), CD45.2 (104; Biolegend), PD1 (RMP1–30; Biolegend), LAG3 (C9B7W; eBioscience), TIM3 (RMT3–23; eBioscience), TIGIT (GIGD7; eBioscience), CD244.2 (m2B4; Biolegend), Foxp3 (FJK-16s; eBioscience), Ki67 (B56; BD Biosciences), BrdU (Bu20A; eBioscience) Bcl2 (BCL/10C4; Biolegend), KLRG1 (2F1; eBioscience), Thy1.1 (OX-7; Biolegend), Thy1.2 (30-H12; Biolegend), IFNγ (XMG1.2; Biolegend), TNFα (MP6-XT22; Biolegend), IL2 (JES6–5H4; Biolegend), IL17A (TC11–18H10.1; Biolegend) and GMCSF (MP1–22E9; Biolegend). For human experiments, single cell suspensions were stained with antibodies against CD3 (SP34–2; BD Biosciences), CD4 (RPA-T4; Biolegend), CD8α (RPA-T8; Biolegend), CD45 (H1100; Biolegend), LAG3 (1408; Bristol-Meyers Squibb), ADAM10 (SHM14; Biolegend), ADAM17 (111633; R&D Systems) and Foxp3 (PCH101; eBioscience).

Surface staining was performed on ice for 15 minutes. Dead cells were discriminated by staining with Ghost Viability Dye (Tonbo Biosciences) in PBS. For cytokine expression analysis, cells were activated with 0.1μg/ml phorbol myristate acetate (PMA; Sigma) and 0.5μg/ml Ionomycin (Sigma) in complete RPMI containing 10% FBS and Brefeldin A (BFA; eBioscience) for 4 hours. For intracellular staining of cytokines and transcription factors, cells were stained with surface markers, fixed in Fix/Perm buffer (eBioscience) for 30 min, washed in permeabilization buffer (eBioscience) twice and stained for intracellular factors in permeabilization buffer for 30 minutes on ice. For cleaved caspase-3 staining, cells were incubated with anti-cleaved caspase-3 (D175; Cell Signaling) for 30 minutes and then stained with Alexa Fluor 555 anti-rabbit IgG (Invitrogen) for 30 minutes at 4°C.

For BrdU labelling, mice were injected with BrdU (Sigma) in 0.2ml sterile PBS (100mg/kg body weight) i.p. 12 hours before harvest. Immunostaining for Ki67 (B56; BD Biosciences) and BrdU (Bu20a; Biolegend) was performed using eBioscience Foxp3 staining and BD Cytofix/Cytoperm kits.

For phosphorylated AKT and S6 staining following surface staining, cells were fixed in 1.5% PFA in Fix/Perm buffer (eBioscience) for 15 minutes at room temperature. Cells were washed in permeabilization buffer (eBioscience) twice and stained with pAKT (S473, D9E; Cell Signaling) and pS6 (S235/236, D57.2.2E; Cell Signaling) for 45 minutes on ice.

Cells were sorted on Aria II (BD Biosciences) or analyzed on Fortessa (BD Biosciences), and data analysis was performed on FlowJo (Tree Star).

For negative selection of $CD8^+$ T cells, biotin-conjugated antibodies against the following targets were used: CD4 (RM4–5; Biolegend), CD11b (M1/70; Biolegend), CD11c (N418;

Biolegend), CD16/32 (93; eBioscience), CD19 (6D5; Biolegend), CD25 (PC61; Biolegend), CD49b (DX5; eBioscience), CD105 (MJ7/18; eBioscience), B220 (RA3–6B2; Biolegend), I-Ab (KH74; Biolegend), γδTCR (eBioGL3; eBioscience), Ly-6G/C (RB6–8C5; Biolegend) and Ter119 (TER119; Biolegend).

## Tumor Models

Mice were injected with MC38 colon adenocarcinoma ($5\times10^5$ cells s.c.), B16-F10 or B16-gp100 melanoma ($1.25\times10^5$ cells i.d.). Tumors were measured every 3 days with digital calipers and tumor volume calculated blinded and randomized. Mice were removed from study when tumor growth reached a mean diameter of 1.5cm or when necrosis was observed. A cohort of mice received a secondary MC38 injection ($2.5\times10^5$ cells subcutaneously) on d42, following primary MC38 tumor injection and resection at d12 or sham control animals.

Therapeutic anti-PD1 was administered when tumors were palpable (6 days) and mice received 200μg anti-PD1 (clone G4) or Armenian hamster IgG isotype (Bioxcell) i.p. on day 6, 9 and 12. Tumors, draining and non-tumor draining lymph nodes were collected for analysis on the indicated time-point. TILs were prepared with enzymatic (collagenase IV (Worthington Biochemical) and dispase (StemCell Technologies); both 1mg/ml) and mechanical disruption.

For Amph-vax experiments, mice were injected with B16-gp100 or B16-F10 melanoma ($1.25\times10^5$ cells i.d.). On days 4 and 11, mice were immunized with 20μg Amph-gp100, or Amph-E7 as a control, s.c. at the base of the tail. Mice also received anti-PD1 (clone G4) or Armenian hamster IgG as an isotype control as the therapeutic regimen detailed above. Tumor area was measured with digital calipers over time.

## Adoptive Transfer of pmel cells

$CD8^+$ T cells were negatively selected from spleen and lymph nodes of pmel mice by incubation with a biotin-conjugated antibody cocktail (anti-CD4, CD25, CD11b, CD11c, CD16/32, CD19, CD49b, CD105, B220, Ly6G/C, I-Ab, γδTCR and Ter119) on ice for 15 minutes. Cells were then washed and incubated with Pierce Streptavidin Magnetic beads (ThermoFisher Scientific) on ice for 15 minutes. Cells were placed on a magnet and non-bound cells were extracted resulting in $CD8^+$ T cells with >90% purity. *Lag3*$^{NC.L/L}$ or *Lag3*$^{NC.L/L}$ CD4$^{Cre}$ mice received an adoptive transfer of purified pmel cells ($1\times10^5$ i.v.). The following day, mice were injected with B16-gp100 melanoma ($1.25\times10^5$ cells i.d.) and tumor was measured over time.

## EAE induction and Lymphocyte Isolation

Mice were immunized with 100μg myelin oligodendrocyte glycoprotein ($MOG_{35–55}$; AAPPTEC) peptide emulsified with 500μg Complete Freund's Adjuvant (CFA; Sigma) s.c. in in either flank. Mice received 400ng pertussis toxin (PTX; List Biologicals) i.p. on day 0 and day 2. Mice were monitored daily and EAE clinical signs were scored by the following grades: 0- no disease; 1- limp tail; 2- partial hind limb paralysis; 3- complete hind limb

paralysis; 4- complete hind limb paralysis and partial front limb paralysis; 5- moribund or death. Mice received DietGel 31M (Diet $H_2O$) during disease course.

Single-cell suspensions were prepared by isolating the brain and spinal cord, following perfusion with PBS before tissues were extracted. Tissues were minced and incubated in 1mg/mL Collagenase D (Roche) and 200U/mL DNase I (Sigma) for 45 minutes at 37°C with intermittent vortexing. Tissues were processed through a 70μm filter, washed, and put through a 30%/70% Percoll (GE healthcare) gradient. Cells were spun at 800xg for 30 minutes at room temperature. Single cells were removed from the interface, washed, and used for subsequent analysis.

For cytokine analyses, cells were stimulated with $MOG_{35–55}$ peptide (10μg/ml) for 20 hours with the last 4 hours in the presence of BFA.

***In vivo* metalloprotease inhibition assays.—**Osmotic pumps were placed subcutaneously on the back of the mice. Following surgery, infusion lasted for 14 days at a release rate of 0.25μl/hr. Plasma was collected by bleeding from the submandibular vein after implantation of s.c. Alzet pumps delivering DMSO or GI245023X (Tocris Biosciences) inhibitor (20mg/kg/d). sLAG3 levels were determined in plasma samples by ELISA.

***In vitro* assays.—**Pure populations of splenocytes or lymphocytes were isolated from non-tumor bearing *Foxp3*$^{YFP\text{-}Cre}$, *Lag3*$^{NC.L/L}$, *Lag3*$^{NC.L/L}$CD4$^{Cre}$ or *Lag3*$^{NC.L/L}$E8I$^{Cre.GFP}$ mice, stimulated with plate-bound anti-CD3 (145–2C11; 5μg/ml) and soluble anti-CD28 (37.51; 5μg/ml). For metalloprotease inhibition assays, cells were incubated with varying concentrations of GI245023X (Tocris Biosciences) inhibitor or DMSO as a control. Supernatant was collected and assayed for sLAG3 by ELISA.

## Soluble LAG3 ELISA

For murine sLAG3 quantification by ELISA, C9B7W (5μg/ml) mAb was coated on a 96-well flat bottomed microtiter plate (Fisher Scientific) in carbonate buffer (50mM $Na_2CO_3$, pH10.4) at 37°C for 1 hour. The plates were washed three times with PBS-Tween 20 (0.05%) and then blocked with 1% FBS in carbonate buffer at 4°C overnight. The plates were washed and supernatant or serum was added for 1 hour incubation at 37°C, the plates were washed and incubated with rabbit anti-LAG3-D1 antisera (1:200 dilution) at 37°C for 1 hour. This was followed by three washes and a 1 hour incubation with HRP-conjugated, anti-rabbit IgG secondary Ab (1:2000 dilution; GE Healthcare). Plates were developed with TMB substrate solution (ThermoFisher Scientific) and the reaction was stopped by adding 50μl of 1N $H_2SO_4$. Absorbance was measured by an Epoch microplate spectrophotometer (Biotek Instruments). sLAG3 concentration was calculated using a purified sLAG3 standard curve, as previously described (11). For human sLAG3 quantification, the human LAG-3 DuoSet ELISA kit (R&D Systems) was utilized, following the manufacturer's instructions.

## Quantitative Real-Time PCR

Total RNA was extracted from sorted T cell populations isolated from tumor or peripheral cells of B16-F10 tumor-bearing *Foxp3*$^{Cre\text{-}YFP}$ mice using RNEasy Plus Micro Kit (Qiagen),

according to the manufacturer's instructions. RNA was reversed-transcribed into cDNA via the High Capacity cDNA Reverse Transcription kit (Applied Biosystems), according to the manufacturer's instructions. Quantitative polymerase chain reaction (qPCR) was performed using Bullseye EvaGreen qPCR MasterMix in a total volume of 20μl and detected using a LightCycler 96 (Roche) instrument. The following primer sequences were used for *Adam10* (Forward Primer: 5'-GCAAAGGAAGGGATATGCAA and Reverse Primer: 5'-ATAGAACCTGCACATTGGCC) and *Hprt* (Forward Primer: 5'-CAGTACAGCCCCAAAATGGTTA and Reverse Primer: 5'-AGTCTGGCCTGTATCCAACA).

## Single-cell RNAseq

**Generation of single-cell RNAseq libraries:** Live $CD4^+/CD8\alpha^+/CD8\beta^+$ T cells were sorted from MC38 tumors of three mice and pooled for each experimental condition. Single-cell libraries were generated from sorted cells using the Chromium Single Cell 3' Reagent (V2 chemistry) as previously described (33). Briefly, sorted cells were re-suspended in PBS with 0.04% bovine serum albumin (BSA; Sigma) and were loaded into parallel lanes for droplet generation in the 10X Controller targeting a recovery of 2,000 cells per sample. After partitioning into droplets, cells were lysed and reverse transcription was performed within droplets. Following reverse transcription, cDNA was isolated and amplified in bulk with 12 cycles of PCR. Amplified cDNA was then selected by SPRIselect beads, fragmented, and adaptors were ligated. Sample indices were then added by PCR, and samples were once again selected using SPRIselect beads. Concentration of libraries were then determined by PCR using KAPA DNA Quantification.

**Sequencing of single cell libraries:** Following generation and quantification of single cell libraries, samples were diluted to 2nM and pooled for downstream sequencing on a NextSeq500 at the Health Sciences Sequencing Core at the UPMC Children's Hospital of Pittsburgh. Samples were run using NextSeq 500/550 high-output v2 kits (150 cycles) with the following parameters: Read 1: 26 cycles; i7 Index: 8 cycles, Read 2: 98 cycles.

**Demultiplexing, alignment and generation of gene/barcode matrices:** Data from the sequencing runs were processed through the CellRanger pipeline (10X Genomics) for demultiplexing and alignment using the mouse reference genome mm10, followed by generation of filtered gene/barcode matrices. Gene/barcode matrices were then further filtered at both the cell- and gene-level. For cell-level filtering, cell barcodes with fewer than 200 or greater than 10,000 unique molecular identifiers (UMIs) were removed. For gene-level filtering, genes were filtered such that only those expressed at level of at least 1 UMI counts in 1% of cells were retained. These cell- and gene-level filtered gene/barcode matrices were then used for downstream analysis.

**Integration of data across samples:** To perform a unified analysis of single-cell RNAseq datasets, we used a data integration workflow recently implemented in Seurat v3 (34). Briefly, this approach aligns datasets by first performing canonical correlation analysis (35) to embed cells in a shared space, followed by mutual nearest neighbor analysis (36) to

identify similar cells across datasets. These “anchors” are then used to align datasets. We used this approach to align each genotype into a unified analysis.

**Visualization, clustering and identification of immune lineages:** After integrating our datasets, we scaled the combined aligned data and performed principal component analysis, heuristically selecting significant principal components for downstream analysis. To visualize our data, we used a fast-Fourier transform accelerated interpolated based t-distributed stochastic neighbor embedding (FItSNE) (19) to embed cells in two dimensions. Clustering was performed using our recently described deterministic annealing Gaussian mixture model clustering (DRAGON) algorithm (37). T cell subpopulations were identified based on expression of canonical markers (i.e. $CD4^+$ $T_{conv}$: *Cd3d*$^+$, *Cd4*$^+$, *Cd8a*$^-$, *Foxp3*$^-$; $CD4^+$ $T_{reg}$: *Cd3d*$^+$, *Cd4*$^+$, *Cd8a*$^-$, *Foxp3*$^+$; $CD8^+$ T cells: *Cd3d*$^+$, *Cd8a*$^+$, *Cd4*$^-$, *Foxp3*$^-$) in clusters.

**Quantifying differences in immune populations between conditions:** We next quantified the magnitude of the differences in each immune population between genotypes and treatment conditions. To accomplish this, we assessed the Bhattacharyya distance (BD) between subsets of cells from each sample unique sample (i.e. genotype and treatment) as recently described (37). Briefly, we compared the BD between subsets of 100 randomly selected cells from each sample for pair of genotype/treatment combinations for each cell type 50 times. We repeatedly subsample cells to empirically determine the distribution of cells with a sample. We also compared the BD between two sets of 100 randomly selected cells for each cell type from the entire dataset to generate a background distribution for comparison.

**Clustering of subpopulations:** To characterize more subtle differences in each T cell subpopulation, we bioinformatically isolated and re-clustered each T cell subset using the data integration approach described above. DRAGON was once again used to identify clusters within the independent analysis of each of the T cell subsets.

**Determining sample enrichment across clusters:** To determine the relationship between samples and clusters, we sought to evaluate the frequency of cells from a given genotype/phenotype present in each cluster while controlling for different numbers of cells present from each sample type and within each cluster. We did this by first dividing the number of cells within a cluster from a given sample by the total number of cells in the dataset from that given sample. We then scaled these values within each cluster by subtracting the mean and dividing by the standard deviation for each cluster, yielding normalized and scaled frequencies of samples in each cluster.

**Differential gene expression analysis:** Differentially expressed genes were determined by comparing the fold-change in expression in a cluster versus all other clusters using a Wilcoxon rank-sum test, as implemented in Seurat v3. (34).

**Gene set enrichment analysis:** To determine whether there was statistically significant enrichment of known gene sets across clusters, we utilized a gene set enrichment analysis based on the competitive gene set enrichment test CAMERA (38), implemented in our

recently described R package “singleseqgset” (37). The curated Reactome gene sets (C2:CP:REACTOME) for *Mus musculus* were downloaded from the Molecular Signatures Database using the “msigdbr” R package. P-values of <0.05 were considered statistically significant.

### Statistical methods

Statistical analyses were conducted using Prism Version 7 (GraphPad). Tumor growth and EAE clinical score over time was analyzed using two-way ANOVA with multiple comparisons (Fig. 1F and 3F; fig. S2A and B, S3A, C and D, S8A, S9B and S10A). Event-free survival was calculated with the Log-Rank (Mantel-Cox) test applied to Kaplan-Meier survival function estimates to determine statistical significance (Fig. 1D to F, 3B, 4B and 5F; fig. S9A and S16E). Comparisons of independent samples were conducted using the Mann Whitney Test (Fig. 3C to E and 4C to E; fig. S8B to E, G and H, S9D to G, S10B to G and S11B). Comparisons of independent samples were conducted using unpaired t-test (Fig. 3G and H, 5A and D; fig. S1F and G, S2C to M, S12A to F, S13A to L, S14D and E, S15A to I and M to O, and S16A and B). Comparisons of paired samples were conducted using Wilcoxon matched pair test (Fig 5C; fig. S14A to C, F to H, K and L). Optimal cutpoints of survival predictors (Fig. 5F and fig. S16E) were selected by recursive partitioning with a minimum group size of 5, using the rpart() package for R version 3.3.1 (R Foundation for Statistical Computing, Vienna, Austria). “n” represents the number of mice or human subjects used in an experiment, with number of individual experiments listed in the legend. Samples are shown with the mean with or without error bars indicating standard error of the mean (s.e.m). Significance was defined as p=0.05.

## Supplementary Material

Refer to Web version on PubMed Central for supplementary material.

## Acknowledgements:

We would like to thank the Vignali lab for all their constructive comments and advice during this project. We thank L. Chen for providing the hybridoma producing the antibody against PD1 (anti-PD1, G4), A. MacIntyre, D. Falkner, N. Sheng and H. Shen from the Immunology Flow Core for cell sorting and the staff of the Division of Laboratory Animal Services for the animal husbandry.

**Funding:** This study was supported by the NIH (P01 AI108545 and R01 AI144422 to D.A.A.V, and EB022433 to D.J.I.). This research was supported in part by the University of Pittsburgh Center for Research Computing through the resources provided. This work benefitted from SPECIAL BD LSRFORTESSATM used the University of Pittsburgh School of Medicine Unified Flow Core funded by NIH S10 OD011925–01.

**Competing interests:** D.A.A.V. has served on scientific advisory boards for Tizona, Oncorus, Werewolf, F-Star and Pieris, and consultancy for Crescendo, Intellia, MPM, Onkaido and Servier. D.A.A.V. holds stock with TTMS, Potenza, Tizona, Oncorus and Werewolf. D.A.A.V. and C.J.W. have submitted patents related to LAG3 that are pending or granted, and are entitled to a share in net income generated from licensing of these patent rights for commercial development. D.A.A.V. and C.J.W. are inventors on issued patents (US [8,551,481]; Europe [1897548]; Australia [2004217526], Hong Kong [1114339]) held by St. Jude Children’s Research Hospital and Johns Hopkins University that cover LAG3. D.A.A.V holds additional patents licensed with Tizona, Bristol-Meyers Squibb and Potenza/Astellas.

D.J.I. holds patents related to the peptide vaccine technology used in the study. He is a consultant and holds equity in Elicio Therapeutics, which has licensed this technology.

## References


1. Gettinger S, Rizvi NA, Chow LQ, Borghaei H, Brahmer J, Ready N, Gerber DE, Shepherd FA, Antonia S, Goldman JW, Juergens RA, Laurie SA, Nathan FE, Shen Y, Harbison CT, Hellmann MD, Nivolumab Monotherapy for First-Line Treatment of Advanced Non-Small-Cell Lung Cancer. Journal of clinical oncology : official journal of the American Society of Clinical Oncology 34, 2980–2987 (2016). [PubMed: 27354485]
2. Topalian SL, Sznol M, McDermott DF, Kluger HM, Carvajal RD, Sharfman WH, Brahmer JR, Lawrence DP, Atkins MB, Powderly JD, Leming PD, Lipson EJ, Puzanov I, Smith DC, Taube JM, Wigginton JM, Kollia GD, Gupta A, Pardoll DM, Sosman JA, Hodi FS, Survival, durable tumor remission, and long-term safety in patients with advanced melanoma receiving nivolumab. Journal of clinical oncology : official journal of the American Society of Clinical Oncology 32, 1020–1030 (2014). [PubMed: 24590637]
3. Hamid O, Robert C, Daud A, Hodi FS, Hwu WJ, Kefford R, Wolchok JD, Hersey P, Joseph RW, Weber JS, Dronca R, Gangadhar TC, Patnaik A, Zarour H, Joshua AM, Gergich K, Elassaiss-Schaap J, Algazi A, Mateus C, Boasberg P, Tumeh PC, Chmielowski B, Ebbinghaus SW, Li XN, Kang SP, Ribas A, Safety and tumor responses with lambrolizumab (anti-PD-1) in melanoma. The New England journal of medicine 369, 134–144 (2013). [PubMed: 23724846]
4. Topalian SL, Hodi FS, Brahmer JR, Gettinger SN, Smith DC, McDermott DF, Powderly JD, Carvajal RD, Sosman JA, Atkins MB, Leming PD, Spigel DR, Antonia SJ, Horn L, Drake CG, Pardoll DM, Chen L, Sharfman WH, Anders RA, Taube JM, McMiller TL, Xu H, Korman AJ, Jure-Kunkel M, Agrawal S, McDonald D, Kollia GD, Gupta A, Wigginton JM, Sznol M, Safety, activity, and immune correlates of anti-PD-1 antibody in cancer. The New England journal of medicine 366, 2443–2454 (2012). [PubMed: 22658127]
5. Turnis ME, Andrews LP, Vignali DA, Inhibitory receptors as targets for cancer immunotherapy. European journal of immunology 45, 1892–1905 (2015). [PubMed: 26018646]
6. Woo SR, Turnis ME, Goldberg MV, Bankoti J, Selby M, Nirschl CJ, Bettini ML, Gravano DM, Vogel P, Liu CL, Tangsombatvisit S, Grosso JF, Netto G, Smeltzer MP, Chaux A, Utz PJ, Workman CJ, Pardoll DM, Korman AJ, Drake CG, Vignali DA, Immune inhibitory molecules LAG-3 and PD-1 synergistically regulate T-cell function to promote tumoral immune escape. Cancer research 72, 917–927 (2012). [PubMed: 22186141]
7. Andrews LP, Marciscano AE, Drake CG, Vignali DA, LAG3 (CD223) as a cancer immunotherapy target. Immunological reviews 276, 80–96 (2017). [PubMed: 28258692]
8. Andrews LP, Yano H, Vignali DAA, Inhibitory receptors and ligands beyond PD-1, PD-L1 and CTLA-4: breakthroughs or backups. Nature immunology 20, 1425–1434 (2019). [PubMed: 31611702]
9. LA OR, Tai L, Lee L, Kruse EA, Grabow S, Fairlie WD, Haynes NM, Tarlinton DM, Zhang JG, Belz GT, Smyth MJ, Bouillet P, Robb L, Strasser A, Membrane-bound Fas ligand only is essential for Fas-induced apoptosis. Nature 461, 659–663 (2009). [PubMed: 19794494]
10. Lichtenthaler SF, Lemberg MK, Fluhrer R, Proteolytic ectodomain shedding of membrane proteins in mammals-hardware, concepts, and recent developments. The EMBO journal 37, (2018).
11. Li N, Workman CJ, Martin SM, Vignali DA, Biochemical analysis of the regulatory T cell protein lymphocyte activation gene-3 (LAG-3; CD223). Journal of immunology 173, 6806–6812 (2004).
12. Li N, Wang Y, Forbes K, Vignali KM, Heale BS, Saftig P, Hartmann D, Black RA, Rossi JJ, Blobel CP, Dempsey PJ, Workman CJ, Vignali DA, Metalloproteases regulate T-cell proliferation and effector function via LAG-3. The EMBO journal 26, 494–504 (2007). [PubMed: 17245433]
13. Lee PP, Fitzpatrick DR, Beard C, Jessup HK, Lehar S, Makar KW, Perez-Melgosa M, Sweetser MT, Schlissel MS, Nguyen S, Cherry SR, Tsai JH, Tucker SM, Weaver WM, Kelso A, Jaenisch R, Wilson CB, A critical role for Dnmt1 and DNA methylation in T cell development, function, and survival. Immunity 15, 763–774 (2001). [PubMed: 11728338]
14. Seo W, Muroi S, Akiyama K, Taniuchi I, Distinct requirement of Runx complexes for TCRbeta enhancer activation at distinct developmental stages. Scientific reports 7, 41351 (2017). [PubMed: 28150718]
15. Rubtsov YP, Niec RE, Josefowicz S, Li L, Darce J, Mathis D, Benoist C, Rudensky AY, Stability of the regulatory T cell lineage in vivo. Science 329, 1667–1671 (2010). [PubMed: 20929851]

16. Workman CJ, Wang Y, El Kasmi KC, Pardoll DM, Murray PJ, Drake CG, Vignali DA, LAG-3 regulates plasmacytoid dendritic cell homeostasis. Journal of immunology 182, 1885–1891 (2009).
17. Liu H, Moynihan KD, Zheng Y, Szeto GL, Li AV, Huang B, Van Egeren DS, Park C, Irvine DJ, Structure-based programming of lymph-node targeting in molecular vaccines. Nature 507, 519–522 (2014). [PubMed: 24531764]
18. Hanson MC, Crespo MP, Abraham W, Moynihan KD, Szeto GL, Chen SH, Melo MB, Mueller S, Irvine DJ, Nanoparticulate STING agonists are potent lymph node-targeted vaccine adjuvants. The Journal of clinical investigation 125, 2532–2546 (2015). [PubMed: 25938786]
19. Linderman GC, Rachh M, Hoskins JG, Steinerberger S, Kluger Y, Fast interpolation-based t-SNE for improved visualization of single-cell RNA-seq data. Nature methods 16, 243–245 (2019). [PubMed: 30742040]
20. Yanez DC, Ross S, Crompton T, The IFITM protein family in adaptive immunity. Immunology, (2019).
21. Yanez DC, Sahni H, Ross S, Solanki A, Lau CI, Papaioannou E, Barbarulo A, Powell R, Lange UC, Adams DJ, Barenco M, Ono M, D'Acquisto F, Furmanski AL, Crompton T, IFITM proteins drive type 2 T helper cell differentiation and exacerbate allergic airway inflammation. European journal of immunology 49, 66–78 (2019). [PubMed: 30365177]
22. Li L, Wan S, Tao K, Wang G, Zhao E, KLRG1 restricts memory T cell antitumor immunity. Oncotarget 7, 61670–61678 (2016). [PubMed: 27557510]
23. Bos R, Sherman LA, CD4+ T-cell help in the tumor milieu is required for recruitment and cytolytic function of CD8+ T lymphocytes. Cancer research 70, 8368–8377 (2010). [PubMed: 20940398]
24. Moss ML, Bomar M, Liu Q, Sage H, Dempsey P, Lenhart PM, Gillispie PA, Stoeck A, Wildeboer D, Bartsch JW, Palmisano R, Zhou P, The ADAM10 prodomain is a specific inhibitor of ADAM10 proteolytic activity and inhibits cellular shedding events. The Journal of biological chemistry 282, 35712–35721 (2007). [PubMed: 17895248]
25. Deng WW, Mao L, Yu GT, Bu LL, Ma SR, Liu B, Gutkind JS, Kulkarni AB, Zhang WF, Sun ZJ, LAG-3 confers poor prognosis and its blockade reshapes antitumor response in head and neck squamous cell carcinoma. Oncoimmunology 5, e1239005 (2016). [PubMed: 27999760]
26. Moskovitz JM, Ferris RL, Tumor Immunology and Immunotherapy for Head and Neck Squamous Cell Carcinoma. Journal of dental research, 22034518759464 (2018).
27. Ferris RL, Blumenschein G Jr., Fayette J, Guigay J, Colevas AD, Licitra L, Harrington KJ, Kasper S, Vokes EE, Even C, Worden F, Saba NF, Docampo LCI, Haddad R, Rordorf T, Kiyota N, Tahara M, Lynch M, Jayaprakash V, Li L, Gillison ML, Nivolumab vs investigator's choice in recurrent or metastatic squamous cell carcinoma of the head and neck: 2-year long-term survival update of CheckMate 141 with analyses by tumor PD-L1 expression. Oral oncology 81, 45–51 (2018). [PubMed: 29884413]
28. Ferris RL, Blumenschein G Jr., Fayette J, Guigay J, Colevas AD, Licitra L, Harrington K, Kasper S, Vokes EE, Even C, Worden F, Saba NF, Iglesias Docampo LC, Haddad R, Rordorf T, Kiyota N, Tahara M, Monga M, Lynch M, Geese WJ, Kopit J, Shaw JW, Gillison ML, Nivolumab for Recurrent Squamous-Cell Carcinoma of the Head and Neck. The New England journal of medicine 375, 1856–1867 (2016). [PubMed: 27718784]
29. Britton GJ, Ambler R, Clark DJ, Hill EV, Tunbridge HM, McNally KE, Burton BR, Butterweck P, Sabatos-Peyton C, Hampton-O'Neil LA, Verkade P, Wulfing Ch C, Wraith DC, PKCtheta links proximal T cell and Notch signaling through localized regulation of the actin cytoskeleton. eLife 6, (2017).
30. Guy CS, Vignali KM, Temirov J, Bettini ML, Overacre AE, Smeltzer M, Zhang H, Huppa JB, Tsai YH, Lobry C, Xie J, Dempsey PJ, Crawford HC, Aifantis I, Davis MM, Vignali DA, Distinct TCR signaling pathways drive proliferation and cytokine production in T cells. Nature immunology 14, 262–270 (2013). [PubMed: 23377202]
31. Kakugawa K, Kojo S, Tanaka H, Seo W, Endo TA, Kitagawa Y, Muroi S, Tenno M, Yasmin N, Kohwi Y, Sakaguchi S, Kowhi-Shigematsu T, Taniuchi I, Essential Roles of SATB1 in Specifying T Lymphocyte Subsets. Cell reports 19, 1176–1188 (2017). [PubMed: 28494867]
32. Liu P, Jenkins NA, Copeland NG, A highly efficient recombineering-based method for generating conditional knockout mutations. Genome research 13, 476–484 (2003). [PubMed: 12618378]

33. Zheng GX, Terry JM, Belgrader P, Ryvkin P, Bent ZW, Wilson R, Ziraldo SB, Wheeler TD, McDermott GP, Zhu J, Gregory MT, Shuga J, Montesclaros L, Underwood JG, Masquelier DA, Nishimura SY, Schnall-Levin M, Wyatt PW, Hindson CM, Bharadwaj R, Wong A, Ness KD, Beppu LW, Deeg HJ, McFarland C, Loeb KR, Valente WJ, Ericson NG, Stevens EA, Radich JP, Mikkelsen TS, Hindson BJ, Bielas JH, Massively parallel digital transcriptional profiling of single cells. Nature communications 8, 14049 (2017).

34. Stuart T, Butler A, Hoffman P, Hafemeister C, Papalexi E, Mauck WM 3rd, Hao Y, Stoeckius M, Smibert P, Satija R, Comprehensive Integration of Single-Cell Data. Cell 177, 1888–1902 e1821 (2019). [PubMed: 31178118]

35. Butler A, Hoffman P, Smibert P, Papalexi E, Satija R, Integrating single-cell transcriptomic data across different conditions, technologies, and species. Nature biotechnology 36, 411–420 (2018).

36. Haghverdi L, Lun ATL, Morgan MD, Marioni JC, Batch effects in single-cell RNA-sequencing data are corrected by matching mutual nearest neighbors. Nature biotechnology 36, 421–427 (2018).

37. Cillo AR, Kurten CHL, Tabib T, Qi Z, Onkar S, Wang T, Liu A, Duvvuri U, Kim S, Soose RJ, Oesterreich S, Chen W, Lafyatis R, Bruno TC, Ferris RL, Vignali DAA, Immune Landscape of Viral- and Carcinogen-Driven Head and Neck Cancer. Immunity 52, 183–199 e189 (2020). [PubMed: 31924475]

38. Wu D, Smyth GK, Camera: a competitive gene set test accounting for inter-gene correlation. Nucleic acids research 40, e133 (2012). [PubMed: 22638577]

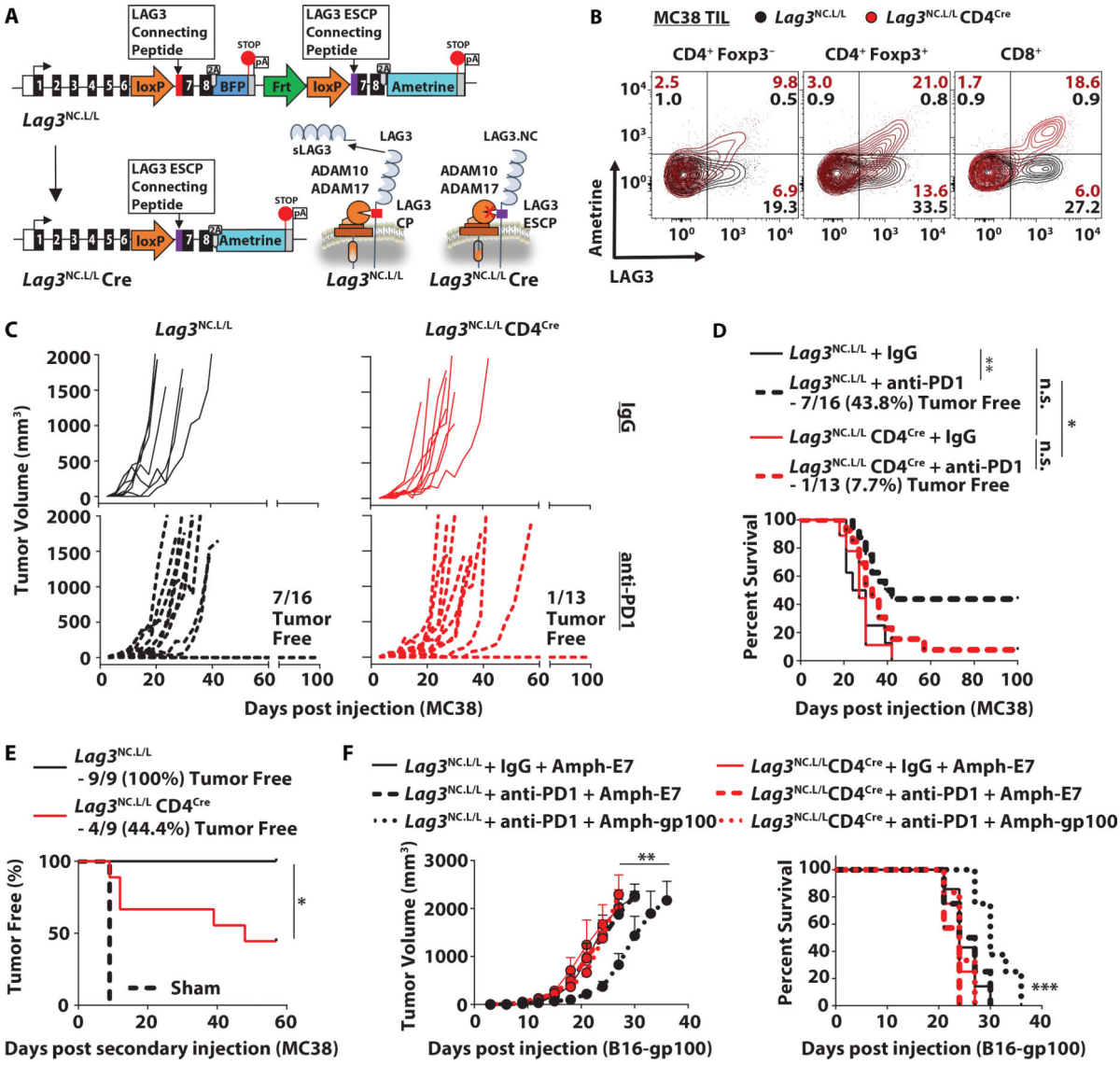


**Figure 1: LAG3$^{NC}$ restricts effective anti-tumor immune responses *in vivo*.**

**(A)** Schematic of LAG3$^{NC}$ conditional knock-in mouse. **(B)** LAG3 and Ametrine expression on CD4$^{+}$ Foxp3$^{-}$, CD4$^{+}$ Foxp3$^{+}$ and CD8$^{+}$ TIL isolated from *Lag3*$^{NC.L/L}$ and *Lag3*$^{NC.L/L}$CD4$^{Cre}$ mice that received 5X10$^{5}$ MC38 adenocarcinoma cells subcutaneously. **(C)** Individual tumor growth curves and **(D)** survival plot of *Lag3*$^{NC.L/L}$ and *Lag3*$^{NC.L/L}$CD4$^{Cre}$ mice receiving 5×10$^{5}$ MC38 adenocarcinoma cells subcutaneously and anti-PD1 or IgG (200μg) on d6, d9 and d12 by intraperitoneal injection. **(E)** Kaplan-Meir curve showing tumor-free animals following secondary MC38 injection (2.5X10$^{5}$ cells subcutaneous) of *Lag3*$^{NC.L/L}$ and *Lag3*$^{NC.L/L}$CD4$^{Cre}$ mice following primary MC38 injection (5X10$^{5}$ cells subcutaneous) and resection (d12), or sham control animals. **(F)** Mean tumor growth curves (left) and survival plot (right) of *Lag3*$^{NC.L/L}$ and *Lag3*$^{NC.L/L}$CD4$^{Cre}$ mice receiving 1.25X10$^{5}$ B16-gp100 melanoma cells intradermally and immunized with Amph-gp100 or Amph-E7 vaccine subcutaneously on d4 and d11 (20μg) with anti-PD1 or IgG as in (C). Results represent the mean of three (B-D) or two (E and F) independent

experiments. *p<0.05, **p<0.01, ***p<0.001, n.s. not significant by (D-F) Log-Rank (Mantel-Cox) and (F) two-way ANOVA. Error bars represent the mean ± s.e.m.

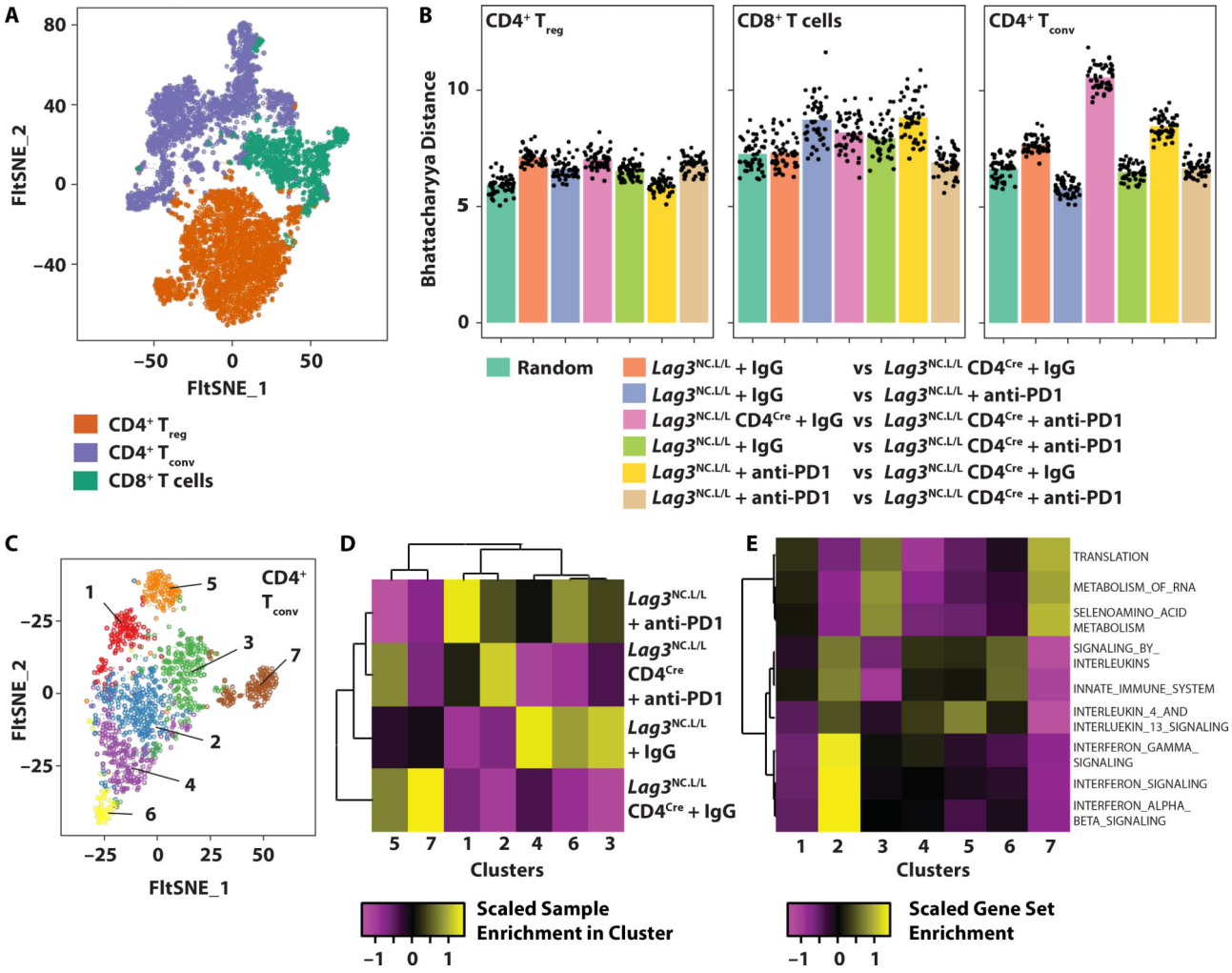


**Figure 2: Single-cell RNAseq analysis of LAG3$^{NC}$-expressing TIL.**

Single-cell RNAseq analysis of T cells isolated from tumors pooled from *Lag3*$^{NC.L/L}$ and *Lag3*$^{NC.L/L}$CD4$^{Cre}$ mice at d14 injected with 5X10$^5$ MC38 adenocarcinoma cells subcutaneously and anti-PD1 or IgG (200μg) on d6, d9 and d12 by intraperitoneal injection. **(A)** FltSNE visualization and DRAGON clustering of all single cells identified CD4$^+$ T$_{reg}$ (red), CD4$^+$ T$_{conv}$ (blue) and CD8$^+$ T cells (green). **(B)** Quantification of differences by Bhattacharyya distance (BD) between CD4$^+$ T$_{conv}$, CD4$^+$ T$_{reg}$ and CD8$^+$ T cells in *Lag3*$^{NC.L/L}$ and *Lag3*$^{NC.L/L}$CD4$^{Cre}$ mice, receiving anti-PD1 or IgG. **(C)** Clustering of CD4$^+$ T$_{conv}$ by DRAGON revealed a total of seven clusters across all samples. **(D)** Scaled sample enrichment in clusters identified in (C). **(E)** Gene set enrichment analysis revealed signature genes associated with each cluster identified in (C).

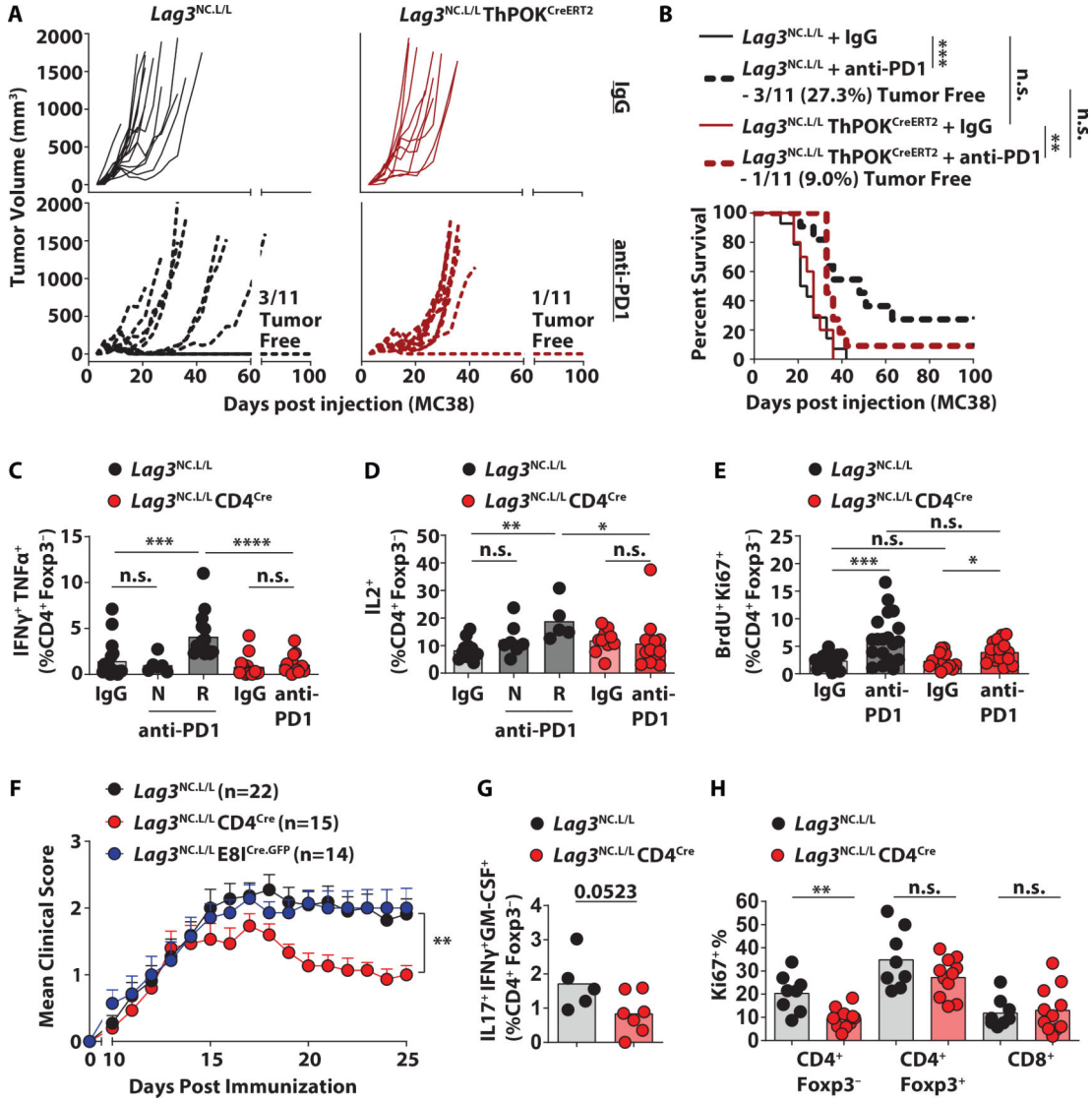


**Figure 3: LAG3$^{NC}$ intrinsically impacts CD4$^{+}$ T cell functionality.**

**(A)** Individual tumor growth curves and **(B)** survival plot of *Lag3*$^{NC.L/L}$ and *Lag3*$^{NC.L/L}$ThPOK$^{CreERT2}$ mice receiving 5X10$^{5}$ MC38 adenocarcinoma cells subcutaneously and anti-PD1 or IgG (200μg) on d6, d9 and d12 by intraperitoneal injection, as well as five consecutive intraperitoneal injections of tamoxifen (1mg in 5% EtOH/ sunflower oil) from d0 to d4. TIL was harvested at d14 from *Lag3*$^{NC.L/L}$ or *Lag3*$^{NC.L/L}$CD4$^{Cre}$ mice injected with 5X10$^{5}$ MC38 adenocarcinoma cells subcutaneously receiving anti-PD1 or IgG (200μg) on d6, d9 and d12 by intraperitoneal injection. **(C)** IFNγ and TNFα, as well as **(D)** IL-2 from CD4$^{+}$ Foxp3$^{−}$ TIL was measured following re-stimulation with phorbol myristate acetate (PMA) and ionomycin for 4 hours in the presence of brefeldin A. Mice that received anti-PD1 were stratified into non-responders (N) and responders (R) to treatment. **(E)** BrdU and Ki67 staining was assessed in CD4$^{+}$ Foxp3$^{−}$ TIL, by intraperitoneal injection of BrdU 12 hours before harvest. **(F)** Mean clinical scores following EAE induction in *Lag3*$^{NC.L/L}$, *Lag3*$^{NC.L/L}$CD4$^{Cre}$ and *Lag3*$^{NC.L/L}$E8I$^{Cre.GFP}$

mice. **(G)** Lymphocytes were isolated from the brain at d14 post immunization and stimulated with $MOG_{35–55}$ peptide for 20 hours and the last 4 hours with Brefeldin A. IL17A, IFN$\gamma$ and GMCSF was assessed from $CD4^+$ $Foxp3^-$ T cells. **(H)** Ki67 was assessed in $CD4^+$ $Foxp3^-$, $CD4^+$ $Foxp3^+$ and $CD8^+$ T cells isolated in (G). Results represent the mean of three independent experiments. *p<0.05, **p<0.01, ***p<0.001, ****p<0.0001, n.s. not significant by (B) Log-Rank (Mantel-Cox), (C-E) Mann Whitney Test, (F) two-way ANOVA and (G and H) unpaired t-test. Error bars represent the mean ± s.e.m.

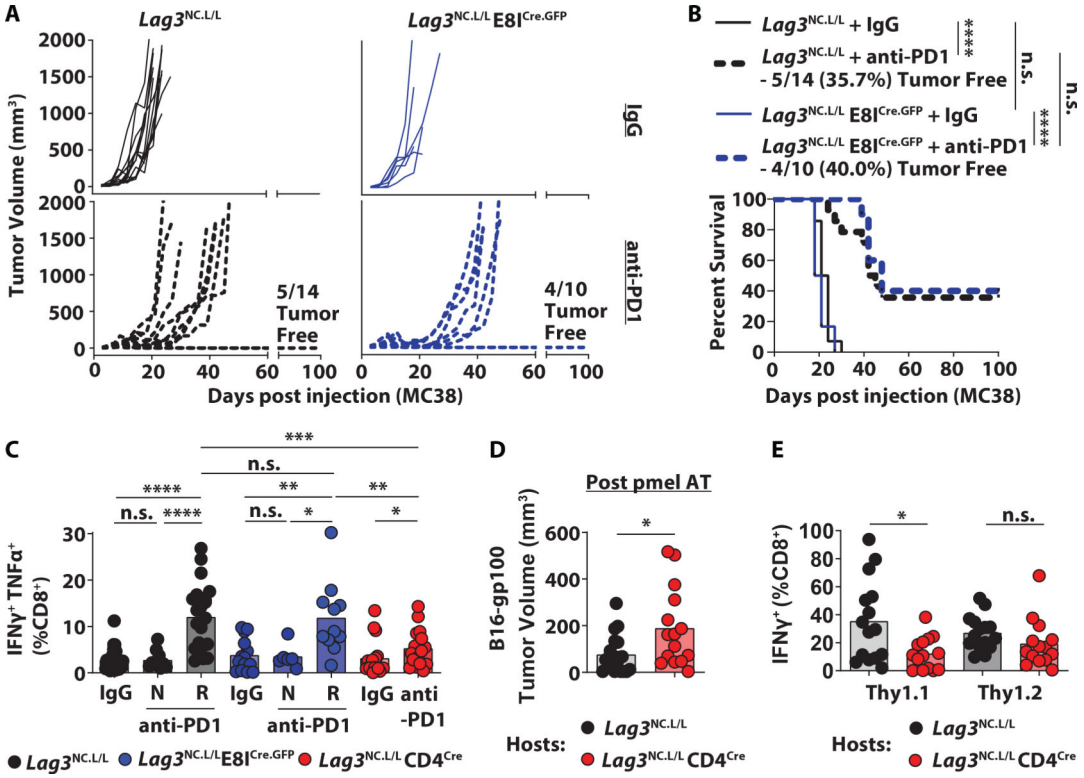


**Figure 4: LAG3$^{NC}$ extrinsically restricts CD8$^{+}$ T cell functionality.**

**(A)** Individual tumor growth curves and **(B)** survival plot of *Lag3*$^{NC.L/L}$ and *Lag3*$^{NC.L/L}$E8I$^{Cre.GFP}$ mice receiving 5X10$^{5}$ MC38 adenocarcinoma cells subcutaneously and anti-PD1 or IgG on d6, d9 and d12 (200μg) by intraperitoneal injection. **(C)** TIL was harvested at d14 from *Lag3*$^{NC.L/L}$, *Lag3*$^{NC.L/L}$CD4$^{Cre}$ or *Lag3*$^{NC.L/L}$E8I$^{Cre.GFP}$ mice injected with 5X10$^{5}$ MC38 adenocarcinoma cells subcutaneously receiving anti-PD1 or IgG (200μg) on d6, d9 and d12 by intraperitoneal injection. IFNγ and TNFα from CD8$^{+}$ TIL was measured following re-stimulation with phorbol myristate acetate (PMA) and ionomycin for 4 hours in the presence of brefeldin A. Mice that received anti-PD1 were stratified into non-responders (N) and responders (R) to treatment. **(D)** *Lag3*$^{NC.L/L}$ or *Lag3*$^{NC.L/L}$CD4$^{Cre}$ mice (Thy1.2$^{+}$) received an adoptive transfer (AT) of 1×10$^{5}$ pmel (Thy1.1$^{+}$) cells the day before inoculation with 1.25X10$^{5}$ B16-gp100 melanoma cells intradermally. Mice received anti-PD1 (200μg) intraperitoneally on d6, d9 and d12 and tumor volume was measured when sacrificed on d15 post inoculation. **(E)** IFNγ was measured on both Thy1.1$^{+}$ (pmel) and Thy1.2$^{+}$ (endogenous) CD8$^{+}$ T cells from (D) following re-stimulation as in (C). Results represent the mean of three independent experiments. *p<0.05, **p<0.01, ***p<0.001, ****p<0.0001, n.s. not significant by (B) Log-Rank (Mantel-Cox) and (C-E) Mann Whitney Test.

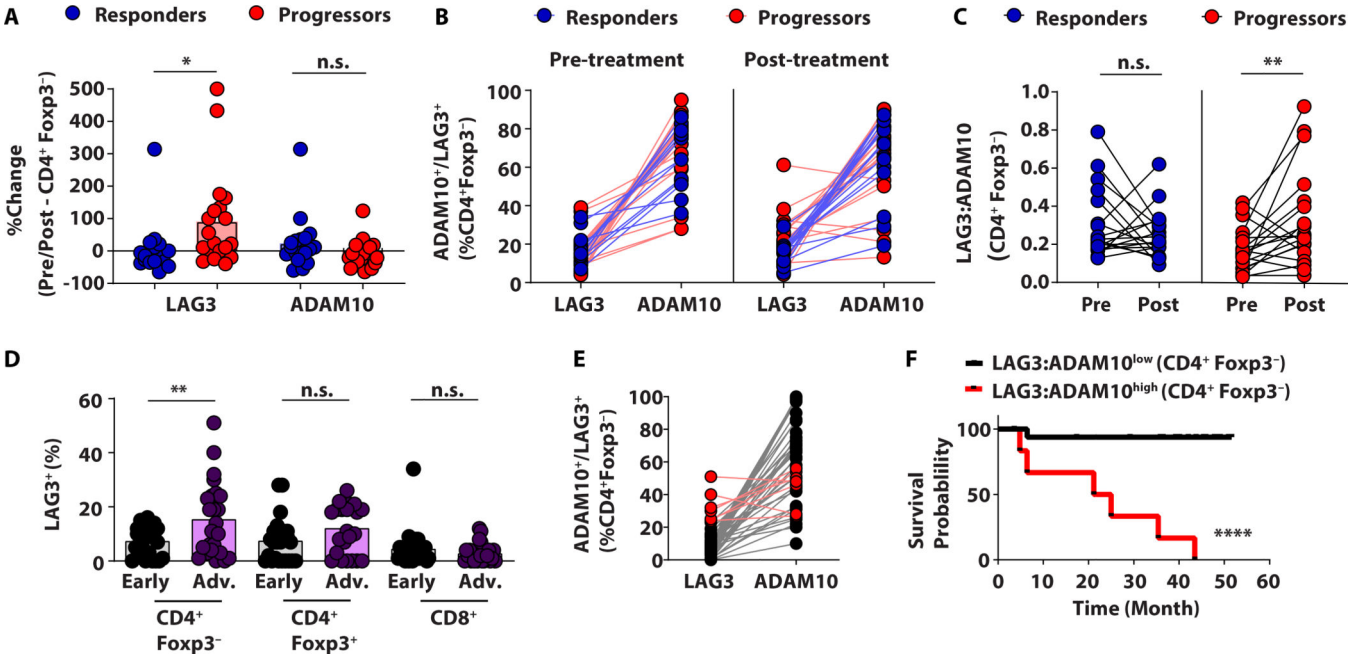


**Figure 5: Low LAG3 and reciprocal high ADAM10 expression on conventional CD4$^+$ T cells is indicative of patient survival and responsiveness to PD1 blockade.**

**(A)** Lymphocytes were isolated from peripheral blood of advanced metastatic melanoma patients prior (pre) or following (post) treatment with standard of care anti-PD1+/−anti-CTLA4 (n=37; Cohort B [Table 3]). The change in LAG3 and ADAM10 expression was assessed for CD4$^+$Foxp3$^-$ T cells and patients were stratified by responsiveness to treatment. **(B)** Paired analysis of LAG3 and ADAM10 expression on CD4$^+$Foxp3$^-$ T cells isolated from patients in (A). **(C)** LAG3:ADAM10 ratio for CD4$^+$Foxp3$^-$ T cells of patients in (A). **(D)** Lymphocytes were isolated from peripheral blood of HNSCC patients (n=50; Cohort D [Table 5]) and LAG3 expression on CD4$^+$Foxp3$^-$, CD4$^+$Foxp3$^+$ and CD8$^+$ T cells was assessed by stage of disease. **(E)** Paired analysis of LAG3 and ADAM10 expression on CD4$^+$Foxp3$^-$ T cells. **(F)** Kaplan-Meier survival curve of advanced disease stage HNSCC patients (n=25) with high LAG3:ADAM10 ratio (±0.3865) or low LAG3:ADAM10 ratio (<0.3865) expressed on CD4$^+$Foxp3$^-$ T cells. *p<0.05, **p<0.01, ****p<0.0001, n.s. not significant by (A and D) unpaired t-test, (C) Wilcoxon Test and (F) Log-Rank (Mantel-Cox).